

Deadlock Resolution and Feasibility Guarantee in MPC-based Multi-robot Trajectory Generation

Yuda Chen, Meng Guo and Zhongkui Li

Abstract—Online collision-free trajectory generation within a shared workspace is fundamental for most multi-robot applications. However, many widely-used methods based on model predictive control (MPC) lack theoretical guarantees on the feasibility of underlying optimization. Furthermore, when applied in a distributed manner without a central coordinator, deadlocks often occur where several robots block each other indefinitely. Whereas heuristic methods such as introducing random perturbations exist, no profound analyses are given to validate these measures. Towards this end, we propose a systematic method called infinite-horizon model predictive control with deadlock resolution. The MPC is formulated as a convex optimization over the proposed modified buffered Voronoi with warning band. Based on this formulation, the condition of deadlocks is formally analyzed and proven to be analogous to a force equilibrium. A detection-resolution scheme is proposed, which can effectively detect deadlocks online before they even happen. Once detected, it utilizes an adaptive resolution scheme to resolve deadlocks, under which no stable deadlocks can exist under minor conditions. In addition, the proposed planning algorithm ensures recursive feasibility of the underlying optimization at each time step under both input and model constraints, is concurrent for all robots and requires only local communication. Comprehensive simulation and experiment studies are conducted over large-scale multi-robot systems. Significant improvements on success rate are reported, in comparison with other state-of-the-art methods and especially in crowded and high-speed scenarios.

Index Terms—Multi-robot systems, motion planning, deadlock resolution, feasibility guarantee.

I. INTRODUCTION

COLLISION-free trajectory generation is essential for multi-robot systems to perform various missions in a shared environment, such as cooperative inspection and transportation [1], [2], [3], [4]. However, it becomes especially challenging when a large number of agile robots navigate in a crowded space with high speed. The commonly-seen multi-robot trajectory generation (MATG) algorithms can be classified into roughly six categories: potential fields [5], [6] that design virtual driving forces induced by artificial potentials; geometric guidance [7], [8] such as reciprocal velocity obstacles (RVO) [8], [9] that analyze the geometric properties based on the position and velocity of the others; conflicts resolution [10], [11] that designs heuristic rules to resolve potential collisions; learning-based methods [12], [13], [14]

that rely heavily on accurate simulators and reward shaping; control-law based methods [15], [16], [17] that have a strong theoretical guarantee; and optimization-based methods [18], [19], [20] that model the problem as numerical optimizations.

Optimization-based methods have gained increasing popularity recently due to its modeling capability and extensibility. In particular, optimization-based methods construct and solve various optimizations to achieve collision-free navigation, such as the mixed integer quadratic programming in [18], sequential convex programming in [21], and model predictive control (MPC) in [22]. However, most of the aforementioned methods do not ensure explicitly feasibility of the underlying optimization during the whole navigation. In other words, the optimization might be infeasible at one time step, thus the whole system stops. Some works in [23], [24] and [25] propose to tackle the feasibility problem by gradually scaling up the time step, which however requires a centralized coordinator. Another work [26] introduces the notion of control barrier function, which can guarantee collision-free trajectory. Nonetheless, it might be overly conservative due to excessive breaking, and often suffers from deadlocks. The methods in [27] ensure feasibility by utilizing relative-safe corridor among robots, which however requires a pre-defined order of optimization among the robots. Last but not least, the above methods often impose a fully-connected communication network with high communication burden.

More importantly, another well-known issue in MATG is that deadlocks often occur during navigation in multi-robot systems. Formally, a deadlock happens when multiple robots are blocked by each other indefinitely and cannot make any progress towards their targets [28]. It is often caused by the symmetric configuration of the underlying system [29], and the lack of a central coordinator [30]. Towards a structured environment where the paths are predefined, several recent works [31], [32] perform well via proper prioritization and scheduling. On the other side, for unstructured environments, the resolution scheme is inspired by the real-life traffic management such as the right-hand rules. For instance, an artificial perturbation to the right-hand side of each robot is introduced in [26] in order to break the equilibrium of deadlock. This however can lead to unpredictable behavior and even safety issue in practice as the magnitude of such perturbations is hard to determine. Other works in [33], [34], [35] instead propose to select a detour point on the right-hand side of each robot as the temporary target. Nonetheless, the validity and effectiveness of these schemes still lack theoretical analyses and guarantee on the performance, and might lead to livelock problems in practice where the robots oscillate around the deadlock positions

This work was supported by the National Natural Science Foundation of China under grants 62203017, 61973006, T2121002, and by Beijing Natural Science Foundation, China under grant JQ20025.

The authors are with the State Key Laboratory for Turbulence and Complex Systems, Department of Mechanics and Engineering Science, College of Engineering, Peking University, Beijing 100871, China. Corresponding author: Zhongkui Li, zhongkli@pku.edu.cn.

indefinitely. Similar clockwise maneuver is adopted in [36] which shows that the tangent motion can resolve deadlocks for some cases. Important advances on deadlock analysis and resolution are recently reported in [29], [37], [38]. The authors in [29], [37], [38] analyze the condition of deadlocks based on the Karush-Kuhn-Tucker (KKT) formulation for multi-robot systems and present a proportional-derivative (PD) control law to resolve deadlock, which unfortunately can be theoretically shown for the case with no more than three robots. As pointed out in [33], algorithms that can provably avoid deadlock in general cases without a global coordinator still await.

To address the open problem of deadlock resolution with feasibility guarantee in a distributed manner, this work proposes a novel systematic trajectory generation method, called infinite horizon model predictive control with deadlock resolution (IMPC-DR). At first, the traditional buffered Voronoi cells (BVC) proposed in [33] is extended greatly by taking into account full planned trajectories of all neighboring robots and introducing a velocity-dependent buffer width. Furthermore, an extra warning band is added to the terminal horizon to facilitate the resolution of potential deadlocks. An improved distributed MPC formulation is proposed based on these constraints and a novel cost function that deals with potential deadlocks. Given this formulation, the condition of deadlocks during navigation is formally analyzed and shown to be analogous to a force equilibrium between the attractive forces from the targets and repulsive forces from the neighboring robots. Consequently, a detection mechanism is designed to detect any potential deadlocks online and before they might happen. Once detected, an adaptive resolution scheme is followed to incrementally adjust the inter-robot repulsive force to break the equilibrium. Properties of the proposed algorithm regarding deadlock resolution, recursive feasibility and local communication are all formally analyzed and proven.

To summarize, the main contributions of this paper are as follows:

- The modified buffered Voronoi cells with warning band (MBVC-WB) introduces a novel trajectory-based and velocity-dependent space partition technique. It can avoid potential collision between the consecutive sampling points, which may take place in the traditional point-based BVC in [33] and the sampling-based methods in, e.g., [22], [39].
- The condition of deadlocks for MPC-based MATG problems is formally analyzed and revealed as a force equilibrium. This is more general than an earlier result in [29] for three robots. Based on this condition, a novel online detection scheme is provided to detect potential deadlocks early-on before they appear, i.e., not afterwards as in [26], [33]. Furthermore, in contrast to heuristic methods in [26], [34], [35], the proposed deadlock resolution scheme has a strong theoretical guarantee that the inter-robot repulsive forces are adapted in a smooth way to falsify the deadlock condition, again before potential deadlocks appear. It is formally proven that under the proposed resolution scheme, no stable deadlocks can exist under minor conditions on the target positions.
- The proposed complete algorithm not only ensures the

property of being deadlock-free, but also guarantees that the optimization at each time step is recursively feasible. Such an assurance for feasibility is often overlooked and simply assumed in related work [21], [40], [41], rather than guaranteed explicitly and formally.

- Effectiveness and performance of the proposed algorithm are validated extensively by numerical simulations against other state-of-the-art methods including iSCP [40], DMPC [41] and BVC [33]. Our method shows a significant increase in both success rate and feasibility, especially for large-scale crowded and high-speed scenarios.
- Hardware experiments are carried out using nano quadrotors Crazyflies in a workspace captured by an indoor motion capture system OptiTrack. Up to 20 nano quadrotors successfully perform experiments of antipodal transitions in 2D and 3D, which further validates the applicability of the proposed algorithms on real-time platforms.

The remaining parts of this paper are organized as follows. Section II describes the problem statement. The method and the corresponding analysis are illustrated in Section III and Section IV, respectively. Section V includes numerical simulations and hardware experiments. Conclusions and future work can be found in Section VI.

II. PROBLEM STATEMENT

This section states formally the multi-robot trajectory generation (MATG) problem considered in this paper.

A. Robot Dynamics

Consider a team of N robots, where each robot $i \in \mathcal{N} \triangleq \{1, 2, \dots, N\}$ is modeled as a point mass in \mathbb{R}^d , and $d = 2, 3$ is the dimension of the configuration space. Furthermore, its motion is approximated by the double integrator, i.e.,

$$\dot{x}^i(t+h) = \mathbf{A}x^i(t) + \mathbf{B}u^i(t)$$

where $x^i(t) = [p^i(t), v^i(t)]$ is robot i 's state, including the position $p^i(t)$ and velocity $v^i(t)$, $u^i(t)$ as acceleration is the control input, $\mathbf{A} = \begin{bmatrix} \mathbf{I}_d & h\mathbf{I}_d \\ \mathbf{0}_d & \mathbf{I}_d \end{bmatrix}$, $\mathbf{B} = \begin{bmatrix} \mathbf{0}_d \\ h\mathbf{I}_d \end{bmatrix}$ and h is the sampling interval. For brevity, the time index “(t)” is omitted wherever ambiguity is not caused in the sequel. As required in practice, both the robot's velocity and acceleration are subjected to physical constraints. Specifically, it holds that $\|\Theta_v v^i\| \leq v_{\max}$ and $\|\Theta_a u^i\| \leq a_{\max}$, where Θ_v, Θ_a are positive-definite matrices, and $v_{\max}, a_{\max} > 0$ denote the maximum velocity and acceleration, respectively.

B. Collision Avoidance

To avoid inter-robot collisions, the minimum distance allowed between any pair of robots is set to $r_{\min} > 0$. In other words, collision is avoided, if

$$\|p^{ij}\| = \|p^i - p^j\| \geq r_{\min} \quad (1)$$

holds, for any pair $(i, j) \in \mathcal{N} \times \mathcal{N}$ and $i \neq j$.

C. MPC-based MATG

The general MATG problem is to design control inputs u^i for each robot $i \in \mathcal{N}$ such that it reaches the target position $p_{\text{target}}^i \in \mathbb{R}^d$, while avoiding collisions with other robots. As discussed in Section I, many existing work adopts the MPC-based solutions, e.g., [18], [22], [42], where the robot trajectories are calculated by solving an optimization problem at each time step and then executed in a receding horizon fashion. At each time step $t \geq t_0$, the planned trajectory of robot i for the future K time steps is defined as $\mathcal{P}^i = [p_1^i, p_2^i, \dots, p_K^i]$ where p_k^i is the planned position for time instant $t + kh$, $k \in \mathcal{K}$; $\mathcal{K} \triangleq \{1, 2, \dots, K\}$ and K is the length of the planning horizon. As a rule of thumb, $K > \frac{v_{\max}}{a_{\max}h}$ is chosen such that the robot can reduce its velocity from maximum to zero within the horizon. Similar notations apply to $v_k^i(t)$, $u_k^i(t)$ as the planned velocity and acceleration. For the ease of notation, $\mathbf{u}^i = [u_0^i, u_1^i, \dots, u_{K-1}^i]$ and analogously for \mathbf{x}^i . Then, the following constrained optimization problem is imposed for the MATG at time $t > t_0$.

Problem 1. At time $t > t_0$, the planned trajectory \mathcal{P}^i of robot $i \in \mathcal{N}$ is the solution to the following optimization:

$$\min_{\{\mathbf{u}^i, \mathbf{x}^i\}} C^i(\mathbf{u}^i, \mathbf{x}^i) \quad (2a)$$

$$\text{s.t. } \|p_k^i - p_k^j\| \geq r_{\min}, \forall j \neq i, \forall k; \quad (2b)$$

$$\mathbf{x}_k^i = \mathbf{A}\mathbf{x}_{k-1}^i + \mathbf{B}\mathbf{u}_{k-1}^i, \forall k; \quad (2c)$$

$$\|\Theta_a \mathbf{u}_{k-1}^i\| \leq a_{\max}, \forall k; \quad (2d)$$

$$\|\Theta_v \mathbf{v}_k^i\| \leq v_{\max}, \forall k; \quad (2e)$$

where $\forall i, k$ is an abbreviation for $\forall i \in \mathcal{N}$ and $\forall k \in \mathcal{K}$; $C^i(\cdot)$ is the cost function to be minimized. ■

Remark 1. The objective function in (2a) can be of various formats, e.g., $C^i = \frac{1}{2} \sum_k (Q_k \|p_k^i - p_{\text{target}}^i\|^2 + R_k \|u_k^i\|^2)$ in [33]. As discussed in the sequel, a novel objective formulation is proposed in this work, which incorporates the deadlock resolution as an integral part of the optimization process. ■

Once this optimization is solved at time t and the planned trajectory is derived, the low-level feedback controller of each robot i tracks $\mathcal{P}^i(t)$ during the time interval $[t, t+h)$. Consequently, it holds that $\mathbf{x}^i(t+h) = \mathbf{x}_1^i(t)$ at time $t+h$. Afterwards, the above optimization is re-formulated given the updated system state, and solved again for the planned trajectory $\mathcal{P}^i(t+h)$. Each robot repeats this procedure locally until *all* robots reach their respective target positions. This is the common framework for most MPC-based MATG methods, see e.g., [43].

D. Distributed Solution, Recursive Feasibility and Deadlock

Notably, constraint (2b) depends on the state of robot j , meaning that the optimization in (2) cannot be solved by robot i alone. However, a *distributed* solution without a central coordinator is desired in this work. In other words, the planned trajectories of all robots are calculated locally by each robot solving the above optimization. Although each robot can only dictate its own trajectory, it can exchange data with other robots via wireless communication to achieve a cooperative

TABLE I
NOMENCLATURES

p_{target}^i	Target of robot i .
p^i, p^{ij}	Position of robot i , $p^{ij} = p^i - p^j$.
p_k^i	Planned position of robot i at the k -th horizon.
\mathcal{P}^i	Planned trajectory of robot i .
$\bar{\mathcal{P}}^i$	Predetermined trajectory of robot i .
\bar{p}_k^i	Position of robot i at the k -th horizon in $\bar{\mathcal{P}}^i$.
v_k^i	Velocity of robot i at the k -th horizon.
x_k^i	$x_k^i = [p_k^i, v_k^i]$.
u_k^i	Control input of robot i at the k -th horizon.
K	Length of horizon.
$\mathcal{K}, \tilde{\mathcal{K}}$	$\mathcal{K} = \{1, 2, \dots, K\}$ and $\tilde{\mathcal{K}} = \{1, 2, \dots, K-1\}$.
w^{ij}	Warning band of robot i w.r.t. robot j .
r_{\min}	The minimum allowable distance between any two robots.
r'_{\min}	$r'_{\min} = \sqrt{r_{\min}^2 + h^2 v_{\max}^2}$.
$\mathcal{N}, \mathcal{N}^i$	The set of all robots, and $\mathcal{N}^i = \{j \mid w^{ij} < \epsilon\}$.
ρ^{ij}	The repulsive coefficient of robot i w.r.t. robot j .
C^i	The objective function of robot i .

strategy. Furthermore, as mentioned previously in Section I, there are two aspects of Problem 1 that are of particular interest in this work: recursive feasibility and deadlock. To be more specific, their exact definitions are stated below.

Definition 1 (Recursive Feasibility). If the optimization in (2) is feasible at time step $t-h$ for each robot $i \in \mathcal{N}$, then the new optimization at time step t remains feasible. ■

Definition 2 (Deadlock). Deadlock happens when all robots are blocked by each other and remain static indefinitely, but at least one robot is *not* at its target position. ■

Recursive feasibility ensures safety of the resulting trajectories, namely no inter-robot collisions would happen. However, for certain configurations such as symmetric and crowded scenarios, the robots may block each other and cannot make progress towards the targets, also known as deadlocks [28]. Although no collisions happen, this case still prohibits a successful navigation. To address these challenges, the main proposed solution is described in the subsequent section, which ensures deadlock resolution with recursive feasibility.

III. PROPOSED SOLUTION

The complete solution is described in this section, which consists of four main steps: re-formulation of the constraint in (2b) for collision avoidance; re-formulation of the complete optimization; formal analyses of the condition for deadlocks; and finally the resolution scheme of potential deadlocks.

A. MBVC-WB

The collision avoidance constraint in (2b) is enforced explicitly by requiring the inter-robot distance to be more than r_{\min} at all time. However, the exact trajectory of other robots are not accessible during planning. Thus, we propose to replace them with the *predetermined trajectory* of other robots.

Definition 3 (Predetermined Trajectory (PT)). The predetermined trajectory for robot i at time t is defined as

$$\bar{\mathcal{P}}^i(t) = [\bar{p}_1^i(t), \bar{p}_2^i(t), \dots, \bar{p}_K^i(t)],$$

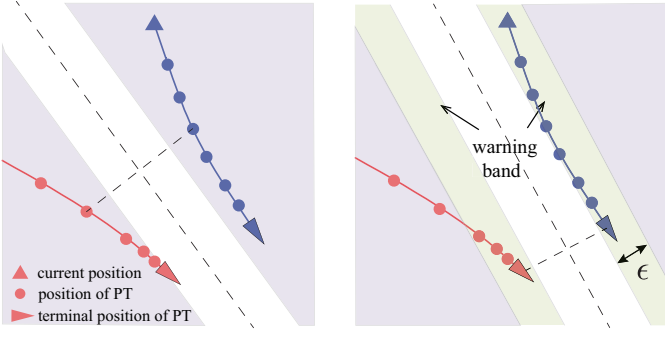


Fig. 1. Illustration of the MBVC-WB. **Left**: the shared space is split at each horizon; **Right**: a warning band is added for the terminal horizon $k = K$.

where $\bar{p}_k^i(t) = p_{k+1}^i(t-h)$, $k \in \tilde{\mathcal{K}} \triangleq \{1, \dots, K-1\}$, and $\bar{p}_K^i(t) = p_K^i(t-h)$ for the terminal horizon. ■

Based on the predetermined trajectory, we use the spatial separation method to handle inter-robot collisions. As illustrated in Figure 1, this method forms a separating hyperplane between different robots which restricts their respective motion space. Inspired by [33], we define the following modified buffered Voronoi cell with warning band (MBVC-WB) for any pair of robots i and j that $j \neq i$:

$$\mathcal{V}_k^{ij} = \left\{ p \mid (p - \frac{\bar{p}_k^i + \bar{p}_k^j}{2})^T \frac{\bar{p}_k^{ij}}{\|\bar{p}_k^{ij}\|} \geq r_k^{ij} \right\}, \quad (3)$$

where \mathcal{V}_k^{ij} is the MBVC-WB for robot i w.r.t. robot j during the horizon $k \in \mathcal{K}$; $\bar{p}_k^{ij} = \bar{p}_k^i - \bar{p}_k^j$; the pair-wise buffer width $r_k^{ij} = \frac{r'_{\min}}{2}$ holds for $k \in \tilde{\mathcal{K}}$, where

$$r'_{\min} = \sqrt{r_{\min}^2 + h^2 v_{\max}^2} \quad (4)$$

is the extended buffer width; and $r_K^{ij} = \frac{r'_{\min}}{2} + w^{ij}$, where w^{ij} is an optimization variable as the warning distance between robots i and j . Note that $0 \leq w^{ij} \leq \epsilon$ with ϵ being the maximum width of the warning band, which is generally chosen as $\epsilon \in (\frac{r_{\min}}{6}, \frac{r_{\min}}{2})$.

Consequently, the collision avoidance constraints between any pair of robots are decoupled and become $p_k^i \in \mathcal{V}_k^{ij}$, $p_k^j \in \mathcal{V}_k^{ji}$. Via simple re-arrangements, the constraint $p_k^i \in \mathcal{V}_k^{ij}$ can be rewritten as

$$a_k^{ijT} p_k^i \geq b_k^{ij}, \quad \forall j \neq i, k \in \tilde{\mathcal{K}}, \quad (5a)$$

$$a_K^{ijT} p_K^i \geq b_K^{ij} + w^{ij}, \quad \forall j \neq i; \quad (5b)$$

where the coefficients are given by

$$a_k^{ij} = \frac{\bar{p}_k^{ij}}{\|\bar{p}_k^{ij}\|}, \quad b_k^{ij} = a_k^{ijT} \frac{\bar{p}_k^i + \bar{p}_k^j}{2} + \frac{r'_{\min}}{2}. \quad (6)$$

Note that the above constraints in (5) can be formulated locally by each robot given the planned trajectory $\mathcal{P}^j(t-h)$ received from its neighbors j at the previous time step $t-h$.

Remark 2. The buffered Voronoi cell (BVC) proposed in [33] is defined as follows:

$$\bar{\mathcal{V}}^{ij} = \left\{ p \mid (p - \frac{p^i + p^j}{2})^T \frac{p^{ij}}{\|p^{ij}\|} \geq \frac{1}{2} r_{\min} \right\}.$$

Compared with the proposed MBVC-WB in (3), there are three main differences: (i) BVC only considers the *current* positions of robots i and j , while MBVC-WB takes into account all future positions of both robots according to their predetermined trajectories. This leads to a more accurate space separation and thus a higher utilization rate of the workspace; (ii) the buffer width r'_{\min} in (4) is velocity dependent to ensure collision avoidance between sampling points; (iii) as explained in the sequel, the warning band w^{ij} added at the terminal horizon K is also included in the objective function, which allows for an effective resolution scheme for potential deadlocks. ■

Lemma 1. If $p_k^i \in \mathcal{V}_k^{ij}$ holds, $\forall i, j \in \mathcal{N}$ that $i \neq j$, and $\forall k \in \mathcal{K}$, then

$$\|p_k^{ij}\| \geq r'_{\min} \quad (7)$$

holds for the same set of i, j, k as above and $p_k^i = p_k^i - p_k^j$. Furthermore, assuming that robots i, j move at constant velocities from p_k^i to p_{k+1}^i and from p_k^j to p_{k+1}^j , respectively, the planned trajectories $\mathcal{P}^i(t)$, $\mathcal{P}^j(t)$ are collision-free over the whole trajectory.

Proof. For robots i and j , if $p_k^i \in \mathcal{V}_k^{ij}$ and $p_k^j \in \mathcal{V}_k^{ji}$ hold for $\forall k \in \mathcal{K}$, it follows that $a_k^{ijT} p_k^j \geq b_k^{ij}$ and $a_k^{jiT} p_k^i \geq b_k^{ji}$, respectively. Hence, $a_k^{ijT} p_k^j + a_k^{jiT} p_k^i \geq b_k^{ij} + b_k^{ji}$ holds. Substituting (6) into it, it follows that $a_k^{ijT} p_k^j \geq r'_{\min}$. Moreover, since $a_k^{ijT} p_k^j \leq \|a_k^{ij}\| \|p_k^{ij}\| \leq \|p_k^{ij}\|$, (7) can be derived. Furthermore, due to (7), it can be shown that

$$\|p_k^{ij}\| \geq r'_{\min} = \sqrt{r_{\min}^2 + h^2 v_{\max}^2}$$

holds for both k and $k-1$. Since the maximum allowed velocity is v_{\max} , it follows that $\|p_k^i - p_{k-1}^i\| \leq h v_{\max}$ and $\|p_k^j - p_{k-1}^j\| \leq h v_{\max}$. Consequently, it yields

$$\begin{aligned} \|p_k^{ij}\| &\geq \sqrt{r_{\min}^2 + h^2 v_{\max}^2} \\ &\geq \sqrt{r_{\min}^2 + \frac{1}{4} \|p_k^i - p_{k-1}^i - p_k^j + p_{k-1}^j\|^2}. \end{aligned}$$

Similarly, it holds that

$$\|p_{k-1}^{ij}\| \geq \sqrt{r_{\min}^2 + \frac{1}{4} \|p_k^j - p_{k-1}^j\|^2}.$$

Given these conditions, Appendix A shows that the inter-robot distance during time $[t + (k-1)h, t + kh]$ is bounded as

$$\|p_{k-1}^i + \beta(p_k^i - p_{k-1}^i) - p_{k-1}^j - \beta(p_k^j - p_{k-1}^j)\| \geq r_{\min} \quad (8)$$

where $\beta \in [0, 1]$. In other words, if robot i moves from p_{k-1}^i to p_k^i and robot j from p_{k-1}^j to p_k^j at constant velocities, according to (8), the minimum distance between robots i and j is larger than r_{\min} for all $k \in \mathcal{K}$. This completes the proof. □

B. Complete Optimization

In addition to the inter-robot collision avoidance, the following terminal constraint is introduced to ensure the feasibility of optimization (2):

$$x_K^i \in X_e, \text{ where } X_e = \{x \mid x = \mathbf{A}x + \mathbf{B}u, u \in \mathbf{U}\}, \quad (9)$$

i.e., X_e is a set of invariant states where feasible inputs exist for the system to remain in these states. For the simple model of double integrator, this terminal constraint (9) is equivalent to $v_K^i = \mathbf{0}_d$.

Remark 3. Note that once the above constraint is enforced, the planning horizon K can be extended to *infinity* as the planned state x_k^i is identical to x_K^i if $u_{k-1}^i = u_e$ where $X_K^i = \mathbf{A}X_K^i + \mathbf{B}u_e$ for $k > K$. Thus it is also called Infinite-horizon MPC (IMPC). Notably, the infinite horizon ensures that the planned trajectory is remained to be collision-free beyond horizon K such that, as the horizon recedes, a feasible trajectory is already prepared. ■

Furthermore, the objective function in (2a) considered in this work consists of two parts:

$$C^i = C_w^i + C_p^i. \quad (10)$$

The first part

$$C_w^i = \sum_{j \neq i} \rho^{ij} \left(\frac{w^{ij}}{\epsilon} - \ln w^{ij} \right) \quad (11)$$

is related to the warning band in (3), $\rho^{ij} > 0$ is a designated parameter for deadlock resolution later. Note that $\lim_{w^{ij} \rightarrow 0^+} C_w^i = +\infty$ and $\frac{\partial C_w^i}{\partial w^{ij}}|_{w^{ij}=\epsilon} = 0$. The second part

$$C_p^i = \frac{1}{2} Q_K \|p_K^i - p_{\text{target}}^i\|^2 + \frac{1}{2} \sum_{k=0}^{K-1} Q_k \|p_{k+1}^i - p_k^i\|^2$$

is similar to the commonly-seen quadratic cost to penalize the distance to target and summed velocity, where Q_k , $k = 0, 1, \dots, K$ are the weighting parameters. In particular, $Q_k > 0$, $k \in \mathcal{K}$ and $Q_0 = 0$. Given the above components, the optimization in (2) is rewritten as follows:

$$\begin{aligned} \min_{\mathbf{u}^i, \mathbf{x}^i, w^{ij}} \quad & C^i \\ \text{s.t.} \quad & a_k^{ijT} p_k^i \geq b_k^{ij}, \forall j \neq i, k \in \tilde{\mathcal{K}}; \quad (12a) \\ & a_K^{ijT} p_K^i \geq b_K^{ij} + w^{ij}, \forall j \neq i; \quad (12b) \\ & \epsilon \geq w^{ij} \geq 0; \quad (12c) \\ & v_K^i = \mathbf{0}_d; \quad (12d) \\ & (2c) - (2e). \end{aligned}$$

where (12a)-(12c) are the re-formulated constraints for collision avoidance and (12d) is the newly introduced terminal constraint; and the objective function C^i is defined in (10).

C. Condition for Deadlocks

Based on Definition 2, when a deadlock happens, the current position p^i and planned positions p_k^i of all robots remain static at their current positions. In other words, $p_k^i(t) = p^i(t_d)$, $\forall k \in \mathcal{K}$ and $\forall t > t_d$, where t_d is the time when a deadlock starts. The following theorem reveals that such deadlocks can only happen under specific conditions.

Theorem 1. Robot $i \in \mathcal{N}$ belongs to a deadlock if the following condition holds:

$$Q_K (p_{\text{target}}^i - p_K^i) + \sum_{j \in \mathcal{N}^i} \rho^{ij} \delta_{ij} a_K^{ij} = 0, \quad (13)$$

where $\mathcal{N}^i \triangleq \{j \mid w^{ij} < \epsilon\}$, $\delta_{ij} = \frac{\epsilon - w^{ij}}{\epsilon w^{ij}}$; and $w^{ij} = w^{ji}$ holds for $j \in \mathcal{N}^i$.

Proof. To begin with, constraint (2c) in (12) can be directly expanded as $x_k^i = \mathbf{A}^k x_0^i + \mathbf{A}^{k-1} \mathbf{B} u_0^i + \dots + \mathbf{B} u_{k-1}^i$, $k \in \mathcal{K}$. Moreover, the domain of w^{ij} in C^i is $w^{ij} > 0$ since $\lim_{w^{ij} \rightarrow 0^+} C_w^i = +\infty$ and C_w^i is only convex when $w^{ij} > 0$. Therefore, the constraints $w^{ij} \geq 0$ can be omitted in (12). Then, the Lagrange function of (12) is given as:

$$\begin{aligned} \mathcal{L}^i = C^i &+ \sum_{k=1}^K u \lambda_k^i (\|\Theta_a u_{k-1}^i\| - u_{\max}) \\ &+ \sum_{k=1}^K v \lambda_k^i (\|\Theta_v v_k^i\| - v_{\max}) \\ &+ \sum_{j \neq i} \lambda_K^{ij} (b_K^{ij} + w^{ij} - a_K^{ijT} p_K^i) + \sum_{j \neq i} w \lambda^{ij} (w^{ij} - \epsilon) \\ &+ \sum_{k=1}^{K-1} \sum_{j \neq i} \lambda_k^{ij} (b_k^{ij} - a_k^{ijT} p_k^i) + t \nu^i v_K^i \\ &+ \sum_{k=1}^K \nu_k^{iT} (x_k^i - \mathbf{A}^k x_0^i - \mathbf{A}^{k-1} \mathbf{B} u_0^i - \dots - \mathbf{B} u_{K-1}^i), \end{aligned}$$

where $u \lambda_k^i$, $v \lambda_k^i$, λ_k^{ij} , $\nu_k^i = [p \nu_k^i, v \nu_k^i]$ and $t \nu^i$ are the Lagrangian multipliers to the corresponding inequality and equality constraints, respectively.

When a deadlock happens, all robots remain static and thus $u_{k-1}^i = \mathbf{0}_d$ and $v_k^i = \mathbf{0}_d$ hold. It implies that both $\|\Theta_a u_{k-1}^i\| < u_{\max}$ and $\|\Theta_v v_k^i\| < v_{\max}$ hold. Hence, according to the complementary slackness condition of Karush-Kuhn-Tucker (KKT) condition [44], $u \lambda_k^i = 0$ and $v \lambda_k^i = 0$ hold. Furthermore, according to the stationary condition of KKT condition, the following equations are satisfied:

$$\frac{\partial \mathcal{L}^i}{\partial p_k^i} = \frac{\partial C^i}{\partial p_k^i} - \sum_{j \neq i} \lambda_k^{ij} a_k^{ij} + p \nu_k^i = 0, \quad (14a)$$

$$\frac{\partial \mathcal{L}^i}{\partial v_k^i} = \begin{cases} v \nu_k^i, & k \in \tilde{\mathcal{K}} \\ v \nu_k^i + t \nu^i, & k = K \end{cases} = 0, \quad (14b)$$

$$\begin{aligned} \frac{\partial \mathcal{L}^i}{\partial u_{k-1}^i} &= -\mathbf{B}^T \mathbf{A}^{T^{K-k}} \nu_K^i - \mathbf{B}^T \mathbf{A}^{T^{K-k-1}} \nu_{K-1}^i \\ &\quad - \dots - \mathbf{B}^T \nu_k^i = 0. \end{aligned} \quad (14c)$$

$$\frac{\partial \mathcal{L}^i}{\partial w^{ij}} = \frac{\partial C^i}{\partial w^{ij}} + \lambda_K^{ij} + w \lambda^{ij} = 0, \quad (14d)$$

Given the actual value of matrices \mathbf{A} , \mathbf{B} , condition (14c) can be rewritten as

$$\nu_K^{iT} \mathbf{A}^{K-k} \mathbf{B} + \nu_{K-1}^{iT} \mathbf{A}^{K-k-1} \mathbf{B} + \dots + \nu_k^{iT} \mathbf{B} = 0, \quad (15)$$

which directly implies that $\nu_K^{iT} \mathbf{B} = 0$, i.e., $[p \nu_K^{iT}, v \nu_K^{iT}]^T \begin{bmatrix} 0 \\ \mathbf{I}_d \end{bmatrix} = 0$ and $v \nu_K^i = 0$. Combined with condition (14b), $v \nu_k^i = 0$, $k \in \mathcal{K}$ holds. Then, (15) can be further simplified as

$$(K-k) h^p \nu_K^i + (K-k-1) h^p \nu_{K-1}^i + \dots + h^p \nu_{k+1}^i = 0.$$

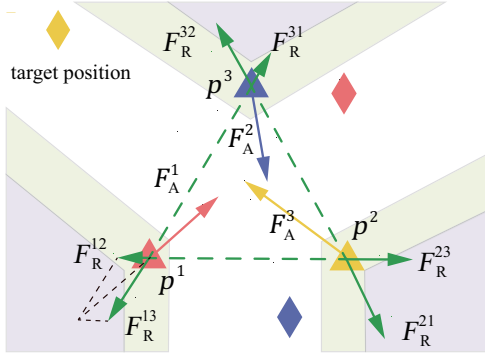


Fig. 2. Deadlock can be treated as a force equilibrium, where the attractive force from the target (in yellow, red, blue) and the repulsive forces from other robots (in green) are balanced.

By setting $k = K - 1$, it follows that $p_{\nu_K}^i = 0$. Consequently, (14a) implies that

$$\frac{\partial \mathcal{L}^i}{\partial p_K^i} = \frac{\partial C^i}{\partial p_K^i} - \sum_{j \neq i} \lambda_K^{ij} a_K^{ij} = 0. \quad (16)$$

Moreover, by substituting (10) into (14d), it follows that

$$\rho^{ij} \left(-\frac{1}{w^{ij}} + \frac{1}{\epsilon} \right) + \lambda_K^{ij} + w \lambda^{ij} = 0. \quad (17)$$

Assume that there exists $j \neq i$ such that $w \lambda^{ij} > 0$ holds. Due to the complementary slackness, $w^{ij} = \epsilon$ holds. Thus, (17) implies $\lambda_K^{ij} + w \lambda^{ij} = 0$. However, the KKT condition requires that both $w \lambda^{ij} \geq 0$ and $\lambda_K^{ij} \geq 0$ must hold. As a result, it follows that $w \lambda^{ij} = 0$ and $\lambda_K^{ij} = 0$ hold, which contradicts the assumption that $w \lambda^{ij} > 0$. Thus, it holds that $w \lambda^{ij} = 0, \forall j \neq i$. Furthermore, combined with (11) and (14d), it follows that

$$\lambda_K^{ij} = -\frac{\partial C^i}{\partial w^{ij}} = -\rho^{ij} \frac{w^{ij} - \epsilon}{\epsilon w^{ij}}. \quad (18)$$

By substituting (18) into (16) and combining $p_K^i = p_{K-1}^i$, it can be derived that

$$Q_K (p_{\text{target}}^i - p_K^i) + \sum_{j \neq i} a_K^{ij} \rho^{ij} \frac{\epsilon - w^{ij}}{\epsilon w^{ij}} = 0.$$

Moreover, if robot $j \notin \mathcal{N}^i$, then both $w^{ij} = \epsilon$ and $\frac{w^{ij} - \epsilon}{\epsilon w^{ij}} = 0$ hold, which leads to equation (13).

If i is trapped at a deadlock, for robot $j \in \mathcal{N}^i$, it must be stuck at this deadlock as well as i , otherwise, i cannot stay at current position as the change of \bar{p}_K^j and a_K^{ij} . For $j \in \mathcal{N}^i$, since $w^{ij} < \epsilon$ and $w \lambda^{ij} = 0$, from equation (17), it is clear that $\lambda_K^{ij} > 0$ which derives

$$a_K^{ijT} p_K^i = b_K^{ij} + w^{ij} \quad (19)$$

via complementary slackness condition. In a similar way, we can obtain

$$a_K^{jiT} p_K^j = b_K^{ji} + w^{ji}. \quad (20)$$

When deadlock happens for i and j , $a_K^{ij} = \frac{p_K^{ij}}{\|p_K^{ij}\|}$ and $b_K^{ij} = a_K^{ijT} \frac{p_K^i + p_K^j}{2} + \frac{r'_{\min}}{2}$ since $\bar{p}_K^i = p_K^i(t-h) = p_K^i$ and $\bar{p}_K^j = p_K^j(t-h) = p_K^j$ holds. By substituting a_K^{ij} and b_K^{ij} in addition

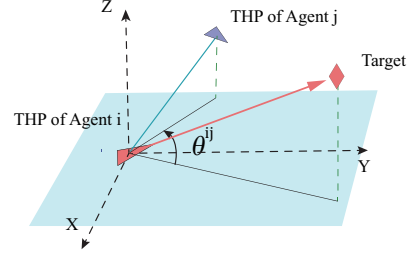


Fig. 3. Illustration of how θ^{ij} in (22) is computed, given the terminal horizon position (THP) of robots i, j and the target.

to combining (19) and (20), $w^{ij} = w^{ji}$ can be finally obtained. This completes the proof. \square

Based on Theorem 1, $F_A^i = Q_K (p_{\text{target}}^i - p_K^i)$ can be regarded as the attractive force from the target and $F_R^{ij} = \rho^{ij} \delta_{ij} a_K^{ij}$ is the repulsive force from robot j , where a_K^{ij} and $\rho^{ij} \delta_{ij}$ are the direction and magnitude, respectively. As illustrated in Figure 2, the deadlock condition (13) can be understood as a balance of these forces, i.e., $F_A^i + \sum_{j \neq i} F_R^{ij} = 0$.

Remark 4. Without the warning band, i.e., $w^{ij} = 0$ and the objective function C^i only includes C_p^i in (10), the necessary condition of deadlocks is rewritten as:

$$Q_K (p_{\text{target}}^i - p_K^i) + \sum_{j \neq i} \lambda_K^{ij} a_K^{ij} = 0, \quad (21)$$

which indicates that the magnitude of the repulsive force λ_K^{ij} will be passively determined. In comparison, after introducing the warning band variable w^{ij} and including it in the objective function (11), the magnitude of the repulsive force satisfies (18) and contains ρ^{ij} as a parameter. Thus, for deadlock resolution, the repulsive forces can be actively adjusted by changing ρ^{ij} , rather than being passively determined as in (21). In other words, via adjusting ρ^{ij} properly, the condition in (13) can be falsified to resolve potential deadlocks. \blacksquare

Remark 5. It should be mentioned that similar analyses based on KKT conditions can be found in [29], [37], [38], which utilizes a control barrier function method. By contrast, the analysis in this theorem is built upon a multi-horizon MPC, and many additional constraints such as (12a)-(12d) and a new term (11) related to the warning band is introduced in the optimization. Furthermore, different from [37], [38], the warning band above provides elastic safety margin when possible deadlock happens. \blacksquare

D. Deadlock Detection and Resolution

A potential deadlock is detected when the following condition termed *terminal overlap* holds.

Definition 4 (Terminal Overlap). The terminal overlap for robot i happens when $p_K^i(t) = p_K^i(t-h)$, $p_K^i(t) \neq p_{\text{target}}^i$, $p_K^i(t) = p_{K-1}^i(t)$, and $p_{K-1}^i(t) = p_{K-2}^i(t)$ hold. \blacksquare

The above condition can be analyzed as follows. According to the condition of deadlocks in (13), the summed forces at the planned terminal position p_K^i equals to zero and remains so

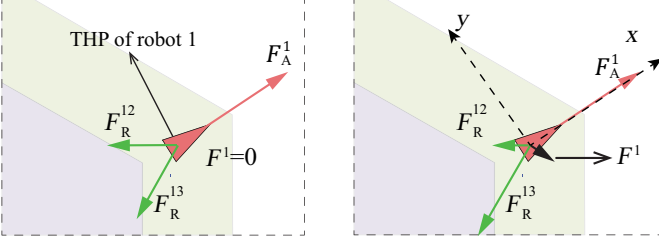


Fig. 4. **Left:** The condition of deadlocks is a force equilibrium for robot 1 in which the resulting force $F^1 = 0$. **Right:** After introducing the right-hand rule, the repulsive force to the left side F_R^13 is increased while the force to the right side F_R^12 is decreased gradually, yielding the summed force F^1 nonzero. Thus the condition of deadlocks is falsified.

indefinitely. Consequently, the planned terminal position at two consecutive time steps are identical, i.e., $p_K^i(t) = p_K^i(t-h)$ holds. Furthermore, the planned positions at the preceding horizons would approach the same position as time evolves and eventually p_K^i overlaps for $k = K, K-1, K-2$. In other words, the condition of terminal overlap above allows an early detection of potential deadlocks by time $(K-2)h$. A duration longer than 2 steps can also be adopted. However, longer duration indicates later detection of deadlocks.

After a positive detection, a resolution scheme is proposed by adapting the coefficient ρ^{ij} as follows:

$$\rho^{ij} = \rho_0 e^{(\eta^i(t) \sin \theta^{ij})},$$

$$\eta^i(t) = \begin{cases} \eta^i(t-h) + \Delta\eta, & \text{if } b_{TO}^i = True; \\ 0, & \text{if } w^{ij} = \epsilon, \forall j \neq i; \\ \eta^i(t-h), & \text{otherwise;} \end{cases} \quad (22)$$

where $\rho_0 > 0$ and $\Delta\eta > 0$ are parameters; initially $\eta^i(t_0) = 0$; $b_{TO}^i = True$ holds when a terminal overlap happens; θ^{ij} is defined as the angle in xy plane between the projection of line \bar{p}_K^i to its target position p_{target}^j and to \bar{p}_K^j , as illustrated in Figure 3.

Consequently, ρ^{ij} is adapted to modify the repulsive forces by following the proposed right-hand rule. Initially, $\rho^{ij} = \rho_0$ and no right-hand forces are introduced. If $b_{TO}^i = True$, η^i is increased and becomes positive. Consider the following two cases: when robot j is on the left-hand side of robot i , i.e., $\theta^{ij} > 0$ and thus $e^{(\eta^i(t) \sin \theta^{ij})} > 1$. As a result, the repulsive force from robot j is increased and thus robot i moves further away from robot j ; Secondly, when robot j is on the right-hand side, robot i approaches to it. Once $w^{ij} = \epsilon, \forall j \neq i$ holds, it is evident that p_K^i must be outside the warning band of any others and there exists no $j \in \mathcal{N}^i$. Then, η^i returns to the initial value 0. Otherwise, η^i remains unchanged.

Remark 6. Compared with other methods proposed in [26], [33], deadlocks can only be detected *after* they happen and thus subsequently resolved “on the spot”. Via the detection mechanism described above, deadlocks can be detected and immediately resolved earlier, *before* they actually happen. As also validated by the numerical results in the sequel, this can lead to a safer and much more efficient navigation scheme, especially in crowded and high-speed scenarios. ■

Algorithm 1: IMPC-DR

Input : $p^i(t_0), p_{target}^i$

- 1 $b_{TO}^i \leftarrow \text{False};$
- 2 $\bar{\mathcal{P}}^i(t_0) \leftarrow \text{InitialPT}(p^i(t_0));$
- 3 **while** not all robots at target **do**
- 4 **for** $i \in \mathcal{N}$ *concurrently* **do**
- 5 $\bar{\mathcal{P}}^j(t) \leftarrow \text{Communicate}(\bar{\mathcal{P}}^i(t));$
- 6 $cons^i \leftarrow \text{MBVC-WB}(\bar{\mathcal{P}}^i(t), \bar{\mathcal{P}}^j(t));$
- 7 $\rho^{ij} \leftarrow \text{DeadlockResolve}();$
- 8 $\mathcal{P}^i(t) \leftarrow \text{Optimization}(cons^i, \rho^{ij});$
- 9 $b_{TO}^i \leftarrow \text{DeadlockDetction}(\mathcal{P}^i(t));$
- 10 $\bar{\mathcal{P}}^i(t+h) \leftarrow \text{GetPT}(\mathcal{P}^i(t));$
- 11 $\text{ExecuteTrajectory}(\mathcal{P}^i(t));$
- 12 $t \leftarrow t+h;$

E. The Complete Algorithm

The complete method is summarized in Algorithm 1. When the system starts, the predetermined trajectory is initialized in Line 2 as $\bar{\mathcal{P}}^i(t_0) = [p^i(t_0), \dots, p^i(t_0)]$. The main loop in Algorithm 1 runs as follows. First, the predetermined trajectory $\bar{\mathcal{P}}^i$ of each robot as defined in Definition 3 is communicated with its neighboring robots in Line 5. Afterwards, the constraints for collision avoidance $cons^i$ in (5) are derived via MBVC-WB in Line 6. Thereafter, the important coefficient ρ^{ij} adopted to the deadlock resolution is obtained. The optimization (12) is formulated with the updated constraints and solved subsequently in Line 8. Based on the result, the boolean variable related to deadlock detection b_{TO}^i is obtained in Line 9. Afterwards, the predetermined trajectory is derived from the planned one via its definition as well. Finally, the planned trajectory is executed by the low-level tracking controller of each robot. The above procedure repeats itself until all robots have reached their target positions.

The computational complexity of the proposed algorithm is analyzed as follows. Since robot i communicates with other robots in \mathcal{N} , its corresponds to $(K+1) \cdot N + K \cdot d$ constraints in (12) and $(K \cdot d + N)$ real variables. The convex programming (12) at each time step can be solved in polynomial time w.r.t. the problem size, e.g., using the interior-point method. Moreover, as shown in the sequel, each robot only needs to communicate with others robot within a certain range, this further reduces the computation complexity above. The complexity of other components, such as the derivation of constraints for collision avoidance and deadlock resolution, are neglected compared with solving the optimization above.

IV. PROPERTY ANALYSES

This section is devoted to the property analyses of the proposed algorithm, regarding deadlocks, feasibility, and local communication.

Theorem 2. Assuming that (i) $\|p_{target}^i - p_{target}^j\| > r'_{min} + 2\epsilon$ holds for $\forall i \neq j$; and (ii) projections of the targets of three or more robots onto the horizontal plane are not collinear, holds, no stable deadlocks exist under Algorithm 1.

Proof. Once the condition of terminal overlap in Definition 4 holds, $\rho^{ij} = \rho_0 e^{(\eta^i(t-h) \sin \theta^{ij})}$ is replaced by $\rho^{ij} = \rho_0 e^{(\eta^i(t) \sin \theta^{ij})}$ where $\eta^i(t) = \eta^i(t-h) + \Delta\eta$. Now consider the direction from robot i to its target position as the x -axis and its orthogonal line as the y -axis, as illustrated in Figure 4. Assume that this deadlock holds indefinitely. By Theorem 1, the summed forces acting on robot i in y -direction are given by

$$F_y^i = \sum_{j \in \mathcal{N}^i} (-\sin \theta^{ij}) \rho_0 e^{(\eta^i(t) \sin \theta^{ij})} \delta^{ij} = 0. \quad (23)$$

Meanwhile, since this deadlock persists and θ^{ij} , δ^{ij} do not change, the equilibrium condition similar to (23) already holds at time $t-h$, i.e.,

$$\sum_{j \in \mathcal{N}^i} (-\sin \theta^{ij}) \rho_0 e^{(\eta^i(t-h) \sin \theta^{ij})} \delta^{ij} = 0. \quad (24)$$

Combining (23) and (24), it follows that

$$F_y^i = \sum_{j \in \mathcal{N}^i} \sin \theta^{ij} (1 - e^{(\Delta\eta \sin \theta^{ij})}) \rho_0 e^{(\eta^i(t-h) \sin \theta^{ij})} \delta^{ij}.$$

Since $\sin \theta^{ij} (1 - e^{(\Delta\eta \sin \theta^{ij})}) \leq 0$ holds for any $\theta^{ij} \in (-\pi, \pi]$, it follows that $F_y^i \leq 0$. Moreover, the equality $F_y^i = 0$ holds if and only if $\theta^{ij} = 0$ or $\theta^{ij} = \pi$ holds, $\forall j \in \mathcal{N}^i$.

Denote by $\mathbb{D}^i = \{j \mid j = i \text{ or } j \in \mathcal{N}^i \text{ or } \exists k \in \mathcal{N}^j, k \in \mathbb{D}^i\}$ the set of robots within the same deadlock of robot i . For robot $j \in \mathbb{D}^i$, it also holds that $\theta^{jk} = 0$ or $\theta^{jk} = \pi$, $\forall k \in \mathcal{N}^j$. In other words, the projections of p_K^j and p_{target}^j onto the xy -plane are collinear, $\forall j \in \mathbb{D}^i$. Since the second condition in Theorem 2 states that the projections of three or more robots' target are not collinear, the analyses can be focused on the case of two robots. Without loss of generality, these two robots are indexed by 1 and 2. By Lemma 3 in the Appendix B, their positions and targets are collinear within a deadlock. Therefore, as depicted in Fig. 5, a new coordinate can be constructed with the line from p_{target}^1 to p_{target}^2 being the x -axis and p_{target}^1 being the origin. In this new coordinate, their positions are denoted by \hat{p}^1 and \hat{p}^2 , and their targets by $\hat{p}_{\text{target}}^1$ and $\hat{p}_{\text{target}}^2$, respectively.

Following Theorem 1, $Q_K(p_{\text{target}}^1 - p_K^1) + \rho^{12} \delta_{12} a_K^{12} = 0$ holds for robot 1; and $Q_K(p_{\text{target}}^2 - p_K^2) + \rho^{21} \delta_{21} a_K^{21} = 0$ holds for robot 2. Additionally, $w^{12} = w^{21}$ and $\delta_{12} = \delta_{21}$ hold. Moreover, since both θ^{12} and θ^{21} are either 0 or π , it holds that $\rho^{12} = \rho_0 = \rho^{21}$. Then, since $a_K^{21} = -a_K^{12}$ holds, $(p_{\text{target}}^1 - p_K^1) + (p_{\text{target}}^2 - p_K^2) = 0$ holds, which leads to the following three cases as shown in Fig. 5.

Case (a): As proven in Lemma 3, the underlying deadlock is unstable.

Case (b): Since $\|p_K^1 - p_K^2\| = \hat{p}^1 - \hat{p}^2 \geq \hat{p}_{\text{target}}^2 - \hat{p}_{\text{target}}^1 > r'_{\min} + 2\epsilon$ holds and w^{12} , $w^{21} \leq \epsilon$, it can be verified that $a_K^{12T} p_K^1 > b_K^{12} + w^{12}$ and $a_K^{21T} p_K^2 > b_K^{21} + w^{21}$ are satisfied. According to complementary slackness condition, this yields that $\lambda_K^{12} = \lambda_K^{21} = 0$ holds. Via (18), this further indicates the repulsive force between robots 1 and 2 are zero, i.e., the robots are attracted by their targets only.

Case (c): Clearly, $\hat{p}^1 \leq \hat{p}_{\text{target}}^1$ and $\hat{p}^2 \geq \hat{p}_{\text{target}}^2$ hold. Thus, similar to the previous case, it implies that $\hat{p}^2 - \hat{p}^1 > r'_{\min} + 2\epsilon$ and the condition for deadlocks cannot hold.

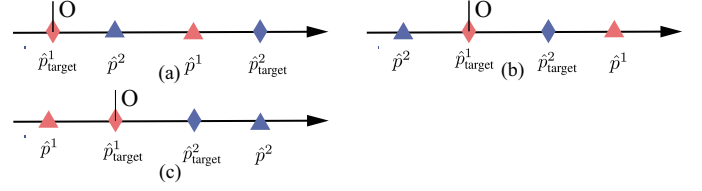


Fig. 5. Illustration of three possible cases when two robots form a deadlock.

To summarize, no stable deadlocks exist under the given two conditions. \square

Remark 7. These two conditions in Theorem 2 are not restrictive as the first condition requires that the targets are at least separated by the minimum safety distance; and the second condition that more than three targets are strictly collinear is quite rare to happen and can be easily avoided by slightly adjusting the target positions. In addition, potential deadlocks can be detected by monitoring θ^{ij} and resolved by applying any arbitrarily small perpendicular force at each robot. Moreover, since deadlocks, if exist, are shown to be unstable, the robots thereby will not return to the previously-resolved deadlock. \blacksquare

Remark 8. The above theorem provides a theoretical guarantee for the proposed deadlock resolution scheme. In comparison, the artificial right-hand perturbation introduced in [26] and the right-hand detour points proposed in [34], [35] are heuristic and thus lacking theoretical analyses. In addition, the above methods in general introduce an instantaneous change of the control inputs whenever deadlocks happen, while the proposed scheme adapts a smooth and gradual adaptation of repulsive forces, before the potential deadlocks actually happen. Moreover, a decentralized control strategy is proposed in [37], [38], which can provably drive the robots out of any possible deadlock. It unfortunately can only be applied to less than three robots and thereby lacks the generality of the proposed deadlock resolution in this paper. \blacksquare

Theorem 3. The optimization in (12) is recursively feasible under Algorithm 1.

Proof. Given a feasible solution $u_{k-1}^i(t-h)$ and $x_k^i(t-h)$ at time $t-h$, $k \in \mathcal{K}$, it is proven in the sequel that $x_k^i(t) = x_{k+1}^i(t-h)$, $u_{k-1}^i(t) = u_k^i(t-h)$, $k \in \mathcal{K}$ and $w^{ij}(t) = \min\{\epsilon, a_K^{ijT}(t)p_K^i(t-h) - b_K^{ij}(t)\}$ is a feasible solution at time t . As mentioned in Remark 3, it is enforced that $x_{K+1}^i(t-h) = x_K^i(t-h)$ and $u_K^i(t-h) = u_e$.

First, as the result of optimization at time step $t-h$, $x_{k+1}^i(t-h)$ and $u_k^i(t-h)$ with $k \in \tilde{\mathcal{K}}$, satisfy the constraints in (2c)-(2e) naturally. In addition, since $x_K^i(t) = x_{K+1}^i(t-h) = x_K^i(t-h)$ and $u_{K-1}^i(t) = u_K^i(t-h) = u_e$ hold, $x_K^i(t)$ and $u_{K-1}^i(t)$ also satisfy these constraints. In the meantime, as $x_K^i(t) = x_{K+1}^i(t-h) = x_K^i(t-h) = x_{K-1}^i(t)$ holds, it is evident that the constraint (12d) holds as well. Second, it has been shown that, by substituting (6), (12a) is equal to

$$\|p_{k+1}^i(t-h) - p_{k+1}^j(t-h)\| \geq r'_{\min}. \quad (25)$$

As a feasible solution at time $t - h$, $p_{k+1}^i(t - h)$ satisfies $a_{k+1}^{ij\top}(t - h)p_{k+1}^i(t - h) \geq b_{k+1}^{ij}(t - h)$, $\forall j \neq i, k \in \tilde{\mathcal{K}}$. Combined with Lemma 1, the inequality in (25) holds as well as constraint (12a). Lastly, it remains to be shown that the constraints in (12b), (12c) and $w^{ij} > 0$ hold. As a feasible solution at time $t - h$, $p_K^i(t - h)$ satisfies $a_K^{ij\top}(t - h)p_K^i(t - h) \geq b_K^{ij}(t - h) + w^{ij}$, for $\forall j \neq i$. Since $w^{ij}(t - h) > 0$ holds, it implies that $a_K^{ij\top}(t - h)p_K^i(t - h) > b_K^{ij}(t - h)$ and further

$$\|p_K^i(t - h) - p_K^j(t - h)\| > r'_{\min}. \quad (26)$$

In addition, since $p_K^i(t - h) = p_{K+1}^i(t - h) = p_K^i(t)$ holds, it yields $\|p_K^{ij}(t)\| > r'_{\min}$. In combination with $a_K^{ij}(t)$ and $b_K^{ij}(t)$ from (6), it is clear that

$$a_K^{ij\top}(t)p_K^i(t) > b_K^{ij}(t). \quad (27)$$

Since $w^{ij}(t) = \min\{\epsilon, a_K^{ij\top}(t)p_K^i(t) - b_K^{ij}(t)\}$, it implies that $w^{ij}(t) > 0$. Thus, the proposed solution $x_k^i(t) = x_{k+1}^i(t - h)$, $u_{k-1}^i(t) = u_k^i(t - h)$, $k \in \mathcal{K}$ and $w^{ij}(t) = \min\{\epsilon, a_K^{ij\top}(t)p_K^i(t) - b_K^{ij}(t)\}$ is a feasible solution at time t . Consequently, the recursive feasibility of optimization (12) is ensured for all robots. \square

Remark 9. It should be mentioned that the infeasible problem in motion planning was considered in previous related work, e.g., [27]. Different from [27] where the planned trajectory is represented by a Bezier-spline, this work considers a more general representation as a sequence of sampled points. Thus, the feasibility results above can be extended to more complex dynamics such as unicycles. More importantly, Theorem 2 together with Theorem 3 demonstrate that the proposed Algorithm 1 indeed solves the deadlock resolution issue with feasibility guarantee. \blacksquare

Corollary 1. *If initially the optimization (12) is feasible, the proposed algorithm ensures that all robots remain collision-free at all time.*

Proof. Since optimization (12) is evidently feasible at $t = t_0$, Theorem 3 shows that it remains feasible for all future time. As an important constraint (12a), the inter-robot collision avoidance is satisfied by any feasible solution. In other words, inter-robot collisions are avoided for all robots at all time. \square

Theorem 4. *The above guarantee for being deadlock-free, collision-free and recursively feasible still holds, if each robot $i \in \mathcal{N}$ only communicates with robot $j \in \mathcal{N}$ that satisfies $\|p^{ij}\| \leq 2v_{\max}Kh + r'_{\min} + 2\epsilon$.*

Proof. To begin with, since $\|p^{ij}\| \geq 2v_{\max}Kh + r'_{\min} + 2\epsilon$ holds, $\|p_k^{ij}\| \geq r'_{\min} + 2\epsilon$ holds, $\forall k \in \mathcal{K}$. Thus, in the case of finite horizon K , there are no repulsive forces between robots i, j , i.e., no deadlocks can appear. Second, constraints might be added or removed in (12) if robots enter or leave the above range, respectively. More specifically, when an existing constraint is removed, its feasibility remains unchanged as the problem is less constrained. On the other hand, a new constraint is added when robot j enters the communication range of robot i . Since $\|p^{ij}\| \geq 2v_{\max}Kh + r'_{\min} + 2\epsilon$ holds, it follows that $\|p_k^{ij}\| \geq r'_{\min}$ holds, $k \in \mathcal{K}$, and in turn (25)

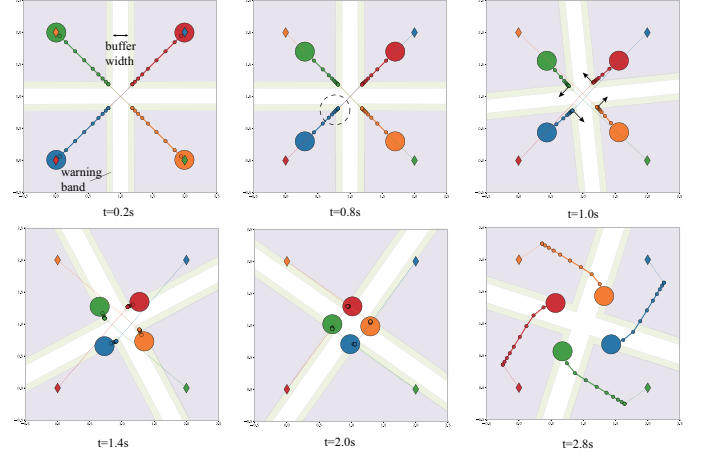


Fig. 6. The process of adopting the proposed right-hand rule where four robots want to swap their positions.

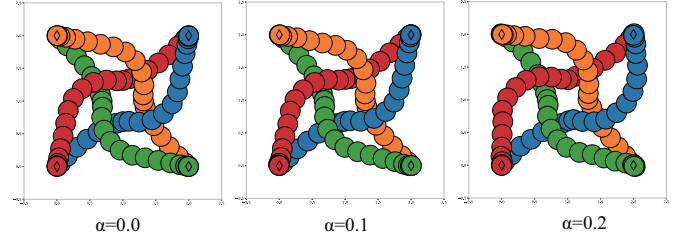


Fig. 7. Trajectories under different disturbances in a symmetric scenario.

holds. Following a similar proof of Theorem 3, it can be shown that $x_k^i(t) = x_{k+1}^i(t - h)$ and $u_{k-1}^i(t) = u_k^i(t - h)$ is a feasible solution as well. Consequently, enforcing the local communication range above does not effect the theoretical guarantee of the complete algorithm on the deadlock-free property and recursive feasibility. \square

Remark 10. Many related work [27], [45] requires a fully-connected communication network. By contrast, the above theorem shows that the proposed algorithm requires a local communication strategy, i.e., each robot only communicates with other robots that are within a communication range. \blacksquare

V. SIMULATION AND EXPERIMENT

In this section, the proposed algorithm is validated via numerical simulations and hardware experiments of large-scale multi-robot systems. The algorithms are implemented in Python3, and publicly available at <https://github.com/PKU-MACDLab/IMPC-DR>. Simulation and experiment videos can be found at <https://youtu.be/IDcXoEer068>. The convex optimizations are formulated by CVXPY [46] and solved by MOSEK [47]. The numerical simulations include some typical scenarios such as symmetric scenarios, narrow passage, position swapping, and random transitions. For the performance evaluation, our method IMPC-DR is compared with three other state-of-the-art methods: iSCP [40], DMPC [41] and BVC [33]. The implementation of iSCP and DMPC is based on [48].

A. Typical Scenarios

To begin with, some typical scenarios in MATG are considered first. To be consistent with the model of UAVs in the experiments, the maximum velocity is set to $v_{\max} = 1.0\text{m/s}$ and the maximum acceleration $a_{\max} = 1.5\text{m/s}^2$. The sampling time h is chosen as 0.2s and the horizon length is set to $K = 10$ for all scenarios. The minimum inter-robot distance r_{\min} is chosen as 0.3m and the width of warning band ϵ is set as 0.1m . In addition, the position penalty is set to $Q_K = 30.0$, $\rho_0 = 2.0$ and $\eta_0 = 2.0$.

1) *Symmetric Scenarios*: Symmetric scenarios are designed such that the initial and target positions of all robots are symmetric, which is the most common cause for deadlocks [29]. As shown in Figure 6, four robots located in a $2\text{m} \times 2\text{m}$ square transit to their antipodal positions. The robots approach the center point initially at $t = 0.2\text{s}$ and the terminal positions have entered the warning band. Then at $t = 0.8\text{s}$, the condition for a terminal overlap holds as the terminal planned positions overlap within the warning band and consequently the proposed resolution scheme is activated. In other words, potential deadlocks are detected at this time instance, before they might happen. As a result, from time $t = 1.0\text{s}$, the robots begin to approach to their right-hand sides, as illustrated in Figure 6. This adaptive process continues at $t = 1.4\text{s}$, 2.0s until the terminal positions leave the warning band and robots have escaped from the deadlock at time $t = 2.8\text{s}$. It is worth noting that without this resolution scheme, a deadlock eventually happens due to the symmetric configuration.

Furthermore, to validate the robustness of our deadlock resolution scheme, artificial forces are applied to all robots as external disturbances, e.g., to mimic wind gust. The forces follow a uniform Gaussian distribution with mean zero and standard deviation σ . As shown in Fig. 7, when $\alpha = \sigma/a_{\max}$ is changed from 0 to 0.2 with the symmetric scenario described above, the proposed navigation and deadlock resolution scheme achieves the same level of deadlock resolution and similar completion time.

2) *Narrow Passage*: The second typical scenario is where a robot needs to pass through another two robots that are already at their respective target positions. This scenario emphasizes the necessity of adding the warning band to the objective function of optimization (12). As shown in Figure 8, via the proposed algorithm, when the robot in the middle approaches the other two robots, these two robots slowly move away from its target position to leave enough space for the middle robot to pass. Concretely, when the middle robot approach to intersection position, another two robots are compelled to enter their warning band related to this robot as shown at $t = 1.4\text{s}$. Intuitively, the penalty term (11) in the objective function (10) can be decreased when both robots on the side move away from their targets until they are not located within the warning band anymore at around $t = 3.0\text{s}$. In contrast, the heuristic approach of choosing a detour point during deadlock suffers from the livelock problem. Specifically, at time $t = 3.0\text{s}$, the robot in the middle chooses a temporary target position and moves away once the deadlock is detected as all robots are static. However, at around $t = 3.4\text{s}$, it judges

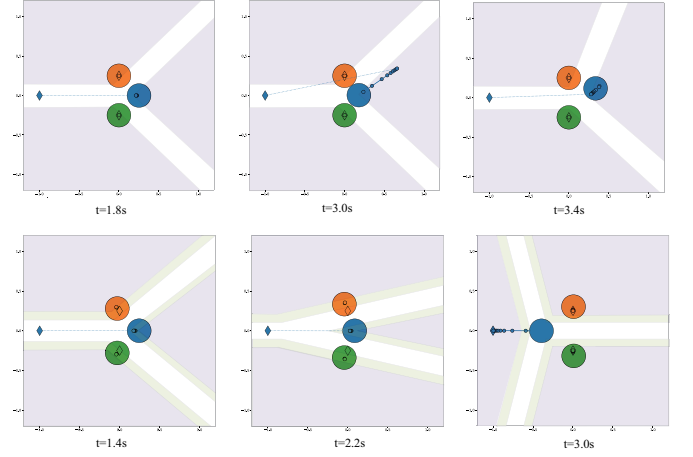


Fig. 8. The typical scenario of narrow passage where one robot passes through other two robots at target positions. **Top**: the traditional right-hand rule suffers from livelock problem. **Bottom**: the proposed method enables the robots on the two sides to temporarily move away and leave space for the middle robot to pass through.

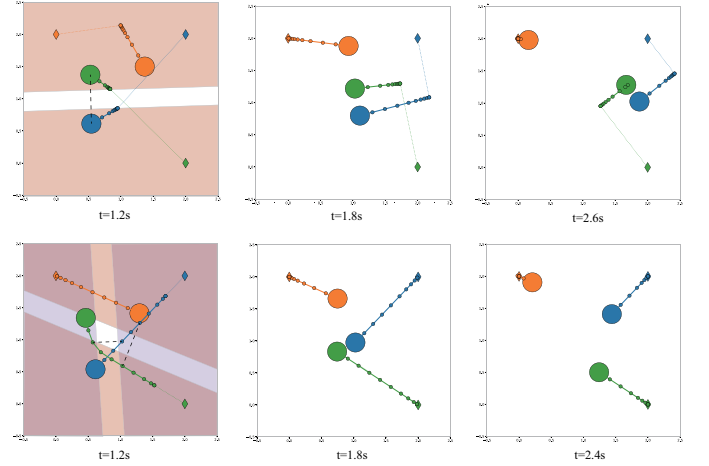


Fig. 9. The typical scenario of swapping positions. **Top**: The traditional BVC method may generate zigzag motions as BVC partitions the workspace only based on the current positions of all robots, as illustrated at $t = 1.2\text{s}$. **Bottom**: The proposed MBVC-WB however divides the workspace based on all future planned trajectories as shown at $t = 1.2\text{s}$. Consequently, much smoother trajectories are generated.

that it has escaped from this deadlock, and the target position is reset to the actual one. Consequently, it comes back to the same deadlock state and this process repeats indefinitely. Similar phenomena can be found if artificial right-hand perturbations [26] are used as the heuristic method.

3) *Position Swapping*: The last scenario is where the robots swap their positions, as shown in Figure 9. This scenario is designed to emphasize that the modified space partition constraint in (5) leads to a more accurate separation among the robots and thus a higher utility rate of the workspace. A comparison between the proposed method and the traditional BVC [33] is shown in Figure 9 for a particular setup. Specifically, since the BVC only considers the current positions of all robots for space partition, all future positions in the planned trajectory are limited to this partition. Thus, it often leads to an overly conservative navigation structure

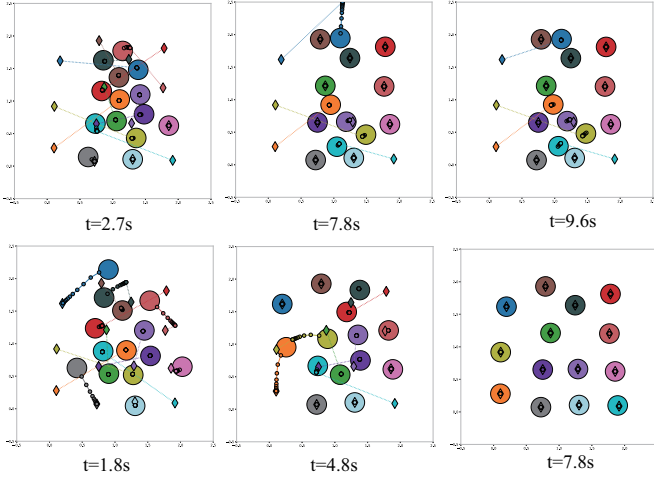


Fig. 10. Snapshots of the random transition in crowded navigation tasks in 2D by 14 robots. **Top:** The traditional right-hand rule that chooses a detour point suffers from the livelock problem, where 4 robots oscillate around the deadlock positions from time $t = 7.8s$. **Bottom:** The proposed method is applied to the same scenario, where potential deadlocks are resolved easily.

with excessive breaking and low efficiency. In contrast, the proposed method enforces multiple space partitions based on the planned positions at each time horizon, i.e., the planned trajectories can be extended as how other robots plan to move. This yields a much smoother and significantly more efficient navigation strategy. This difference is apparent in Figure 9, where the robots accomplish the navigation task via the proposed method at $t = 3.0s$ while it takes $4.0s$ for the traditional BVC method. More detailed comparisons w.r.t. efficiency and success rate can be found in the next part.

B. Random Transitions

To systematically compare our method with other baselines including the incremental sequential convex programming (iSCP) [40], the distributed model predictive control (DMPC) [41] and the buffered Voronoi cell (BVC) [33], the scenario of random transitions is designed, where the initial and target positions are randomly chosen in crowded 2D workspace and high-speed 3D space. In total, 100 random tests are generated for each case. In each test, a navigation task is successful if all robots arrive at their target positions within considerable long time 50.0s. Note that for optimization-based methods, if the underlying optimization is infeasible and thus no solution exists at any time step, then the task fails.

1) *Crowded 2D Workspace:* The 2D workspace is set to $2m \times 2m$ and the number of robots ranges from 2 to 14. The safety diameter, maximum velocity, maximum acceleration, the warning band width and other parameters are selected the same as before. The only difference is that the sampling time $h = 0.15s$ and the horizon length is set to $K = 12$. An example of 14 robots is shown in Figure 10. The results in terms of success rate and infeasibility are summarized in Table II, which shows that IMPC-DR achieves 100% success rate and does not suffer from infeasibility at all. Especially for the highly crowded case of 14 robots, the success rate is much higher than other baselines. More specifically, BVC [33]

TABLE II
RANDOM TRANSITIONS IN CROWDED 2D SCENARIOS

Metric	Method	Number of robots						
		2	4	6	8	10	12	14
Success	IMPC-DR	100	100	100	100	100	100	100
	BVC [33]	100	100	97	94	83	65	41
	iSCP [40]	100	99	94	81	58	39	12
	DMPC [41]	100	99	98	91	95	73	63
Infeas.	IMPC-DR	0	0	0	0	0	0	0
	BVC [33]	0	0	1	0	0	2	0
	iSCP [40]	0	1	6	19	20	61	88
	DMPC [41]	0	1	2	9	5	27	37

TABLE III
TIME OF RANDOM TRANSITIONS IN CROWDED 2D SPACE

Method	Completion Time [s]						
	2	4	6	8	10	12	14
IMPC-DR	1.98	2.28	2.72	3.16	4.31	5.06	6.20
BVC [33]	2.01	2.75	3.26	4.51	6.21	7.97	10.85

with simple right-hand heuristic often suffers from the livelock problem described earlier in Section IV with a success rate only at 41%, of which an example is shown in Figure 10. It is worth noting that when ϵ is set to 0.1m, 14 robots within the finite space of $2m \times 2m$ is almost at the *highest* capacity. One thousand random tests are conducted with a success rate of 100% and zero deadlocks as well as no livelock. This implies that the proposed method in this work has a good performance of deadlock resolution and livelock avoidance. Furthermore, the completion time is evaluated for BVC [33] and the proposed method to illustrate the efficiency of MBVC-WB. As provided in Table III, the proposed method has a significant decrease in transition time especially in a more crowded scenario.

2) *High-Speed 3D Workspaces:* In this case, the maximum velocity and acceleration are increased to $3m/s$ and $2m/s^2$, respectively; the 3D workspace is extended to $10m \times 10m \times 5m$. The safety diameter of all robots is set to 1.0m in addition to the warning band width is extended to 0.2m. As shown in Figure 11, 60 robots can transit at a high speed with safety guarantee by IMPC-DR in this space. Tests are performed for system sizes from 8 to 60, of which the comparisons w.r.t. the success and infeasibility rate are summarized in Table IV. It can be seen that the performance remains almost the same as the 2D case in Table II. In contrast, the performance of other baselines degraded *significantly*, mostly due to aggressive trajectories and slow reaction to deadlocks. This highlights the effectiveness of the proposed terminal constraints in (9).

It is worth pointing out that for the above evaluation, the computation of all robots is performed on one common computer. However, the planning of each robot is an independent process. Despite of being implemented in Python3 instead of C++, it can still achieve a cycle time of 0.75s for the most complex case of 60 robots in 3D. Figure 12 illustrates how the computation time changes as the number of robots increases. It can be seen that the local computation time of each robot

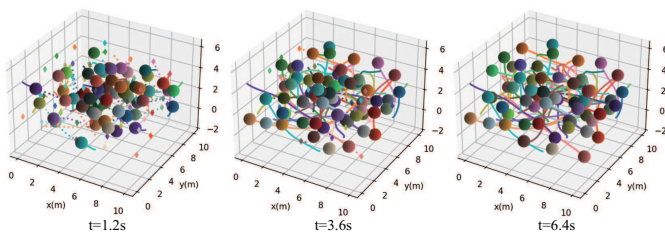


Fig. 11. Snapshots of high-speed random transitions within 3D via the proposed method by 60 robots.

TABLE IV
RANDOM TRANSITIONS IN HIGH-SPEED 3D SCENARIOS

Metric	Method	Number of robots						
		8	16	24	32	40	50	60
Success	IMPC-DR	100	100	100	100	100	100	100
	BVC [33]	95	58	43	35	27	21	17
	iSCP [40]	49	5	0	0	0	0	0
	DMPC [41]	83	36	12	0	0	0	0
Infeas	IMPC-DR	0	0	0	0	0	0	0
	BVC [33]	5	42	57	65	73	79	83
	iSCP [40]	51	95	100	100	100	100	100
	DMPC [41]	17	64	88	100	100	100	100

remains almost unchanged as the system size increases. Thus, the proposed distributed method scales well with the number of robots.

C. Experiments

To further validate the proposed method, several experiments are performed on a nano quadrotor platform.

1) *Hardware Setup*: As shown in Figure 13, the platform consists of several nano quadrotors named Bitcraze Crazyflie 2.1. Their states in the workspace are captured by an indoor motion capture system *OptiTrack*, of which the update frequency is 120Hz. This information is sent to the main control computer where the proposed trajectory generation algorithm is carried out for all quadrotors. The trajectory of quadrotor is fitted to a 7th-order polynomial and then sent to other quadrotors along with its state information via high-frequency radio. After receiving the position information, Kalman filter is used to estimate the current velocity and position. A feedback controller is used to track the updated trajectory based on [49] that ensures a high tracking accuracy.

Furthermore, to avoid the inter-quadrotor air turbulence, the minimum distance between quadrotors r_{\min} is chosen as 0.3m and the width of warning band ϵ is chosen as 0.1m. The maximum velocity and acceleration of Crazyflies are set to 1m/s and 1m/s², respectively, to ensure safety. Lastly, the sampling time h is set to 0.2s and the horizon length to 15, to balance the control performance and the computation burden.

2) *Results*: The first experiment is the symmetry scenario where 20 quadrotors transit to their antipodal position in a 2D circle with radius 1.7m. As shown in Figure 14(a), the navigation task is accomplished within 11.3s with smooth and safe trajectories, where the pattern of right-hand rotation due to the proposed deadlock resolution scheme is apparent. In

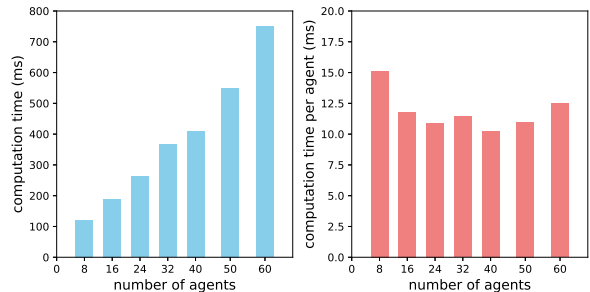


Fig. 12. **Left**: Computation time over different system sizes. **Right**: Computation time per robot.



Fig. 13. Hardware platform consists of a team of Crazyflies nano quadrotors, a motion capture system, and a control computer.

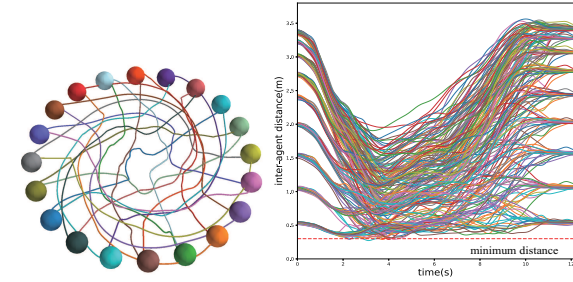
the second experiment, 8 quadrotors transit to their antipodal corners in a cube of 1m³. To consider the downwash effect caused by flying quadrotors, the robots are encapsulated within an ellipsoid of diameter 0.3m in xy -axis and 0.7m in z -axis. The proposed IMPC-DR formulation in (12) can be easily adapted to this configuration. The final trajectories are shown in Figure 14(b), where the right-hand rotation is also visible when the robots avoid each other.

VI. CONCLUSION

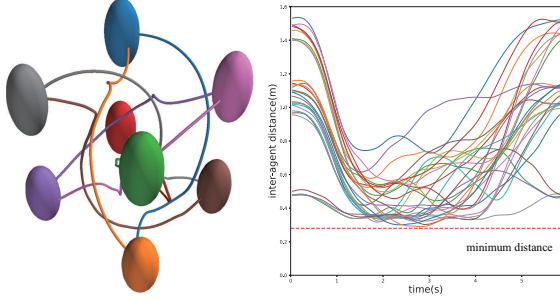
This work has proposed a novel and effective navigation algorithm for multi-robot systems. Its core part is called infinite-horizon model predictive control with deadlock resolution. Different from many heuristic methods, it can effectively detect and resolve deadlocks online before they even happen. In addition, it provably ensures recursive feasibility of the underlying optimization at each time step. It is a fully distributed method that requires only local communication and scales well with the number of robots. Compared with other state-of-the-art baselines, its advantages especially in crowded and high-speed scenarios are significant, as demonstrated both in simulations and hardware experiments. Future work includes the extension to obstacle-rich environments in combination with search-based planning methods.

APPENDIX A LEMMA 2

Lemma 2. Consider two line segments: the line segment from p_1 to p_2 and the line segment from q_1 to q_2 , where



(a) Twenty robots transit to their antipodal positions in a circle. **Left:** Robot Trajectories. **Right:** Inter-robot distances.



(b) 8 crazyflies in a cube fly to their antipodal positions. **Left:** Robot Trajectories. **Right:** Inter-robot distances.

Fig. 14. Hardware experiments of several scenarios, which can be compared with the numerical simulations in Section V-A.

$p_1, p_2, q_1, q_2 \in \mathbb{R}^d$, $d = 2, 3$. If

$$\|r_1\|, \|r_2\| \geq \sqrt{r_{\min}^2 + \frac{1}{4}\|l_2 - l_1\|^2} \quad (28)$$

is satisfied for $r_1 = q_1 - p_1$, $r_2 = q_2 - p_2$, $l_1 = p_2 - p_1$ and $l_2 = q_2 - q_1$, then

$$\|p_1 + t(p_2 - p_1) - q_1 - t(q_2 - q_1)\| \geq r_{\min} \quad (29)$$

holds, $\forall t \in [0, 1]$.

Proof of Lemma 2. It is trivial to show that the left-hand side of (29) is equivalent to

$$p_1 + t(p_2 - p_1) - q_1 - t(q_2 - q_1) = r_1 + t(r_2 - r_1).$$

Hence, it suffices to prove that

$$\|r_1 + t(r_2 - r_1)\| \geq r_{\min}, \quad \forall t \in [0, 1].$$

Let us introduce a function $F(t) = \|r_1 + t(r_2 - r_1)\|^2$, $t \in [0, 1]$. Moreover, set $F(t_{\min}) = \min_{t \in [0, 1]} F(t)$. Consider the following three cases:

- (a) $t_{\min} = 0$: $F(0) = r_1^T r_1 \geq r_{\min}^2$.
- (b) $t_{\min} = 1$: $F(1) = r_2^T r_2 \geq r_{\min}^2$.
- (c) $0 < t_{\min} < 1$: the $F(t_{\min})$ is given by

$$F(t_{\min}) = \frac{r_1^T r_1 r_2^T r_2 - r_1^T r_2 r_1^T r_2}{(r_2 - r_1)^T (r_2 - r_1)},$$

where

$$t_{\min} = -\frac{r_1^T (r_2 - r_1)}{(r_2 - r_1)^T (r_2 - r_1)}. \quad (30)$$

$F(t_{\min}) \geq r_{\min}^2$ is equivalent to

$$r_1^T r_1 r_2^T r_2 - r_1^T r_2 r_1^T r_2 \geq r_{\min}^2 (r_2 - r_1)^T (r_2 - r_1).$$

that can be rewritten as

$$\begin{aligned} & (r_1^T r_1 - r_{\min}^2) (r_2^T r_2 - r_{\min}^2) \\ & \geq (r_1^T r_2 - r_{\min}^2) (r_1^T r_2 - r_{\min}^2). \end{aligned} \quad (31)$$

Now, we consider the following two cases:

- (i) $r_1^T r_2 - r_{\min}^2 \geq 0$. Since $t_{\min} \in (0, 1)$, it follows from (30) that $r_1^T r_1 \geq r_1^T r_2$ and $r_2^T r_2 \geq r_1^T r_2$. Thus,

$$\begin{aligned} r_1^T r_1 - r_{\min}^2 & \geq r_1^T r_2 - r_{\min}^2 \geq 0, \\ r_2^T r_2 - r_{\min}^2 & \geq r_1^T r_2 - r_{\min}^2 \geq 0, \end{aligned}$$

exists which induces (31).

- (ii) $r_1^T r_2 - r_{\min}^2 < 0$. Without loss of generality, we can assume that $r_1^T r_1 \leq r_2^T r_2$. Then, it is easy to show that $r_1^T r_1 \geq r_{\min}^2 + \frac{1}{4}\|l_2 - l_1\|^2$ given (28). It can be further combined with the simple fact that $l_2 - l_1 = q_2 - q_1 - p_2 + p_1 = r_2 - r_1$, which leads to

$$\begin{aligned} r_1^T r_1 & \geq r_{\min}^2 + \frac{1}{4}\|r_2 - r_1\|^2 \\ & = r_{\min}^2 + \frac{1}{4}(r_1^T r_1 + r_2^T r_2 - 2r_1^T r_2) \\ & \geq r_{\min}^2 + \frac{1}{4}(2r_1^T r_1 - 2r_1^T r_2). \end{aligned}$$

After re-organizing the terms, we have

$$r_2^T r_2 \geq r_1^T r_1 \geq 2r_{\min}^2 - r_1^T r_2,$$

and

$$\begin{aligned} r_1^T r_1 - r_{\min}^2 & \geq r_{\min}^2 - r_1^T r_2 \geq 0, \\ r_2^T r_2 - r_{\min}^2 & \geq r_{\min}^2 - r_1^T r_2 \geq 0, \end{aligned}$$

which implies (31).

Now, the proof is completed. \square

APPENDIX B

LEMMA 3

Lemma 3. Via the proposed navigation scheme, if a deadlock is formed by two robots 1 and 2, the following properties hold: 1): p^1 , p_{target}^1 , p^2 and p_{target}^2 are collinear. 2): the deadlock pattern shown in Fig. 5(a) is unstable.

Proof. Since it is proven in Theorem 1 that the summed forces equal to zero, it implies that $a_K^{12} = -\frac{p_{\text{target}}^1 - p_K^1}{\|p_{\text{target}}^1 - p_K^1\|} = -\frac{p_{\text{target}}^1 - p^1}{\|p_{\text{target}}^1 - p^1\|}$. Furthermore, via (6), it holds that $a_K^{12} = -\frac{p_K^1 - p_K^2}{\|p_K^1 - p_K^2\|} = \frac{p^1 - p^2}{\|p^1 - p^2\|}$. Thus, p_{target}^1 , p^1 and p^2 are collinear. Via similar analyses, p_{target}^2 , p^1 and p^2 are also collinear. Consequently, p^1 , p_{target}^1 , p^2 and p_{target}^2 are all collinear.

Second, to show that the deadlock pattern in Fig. 5(a) is unstable, the definition of instability in [50] is followed. Namely, it is proven below that there exists a closed bound \mathcal{B}^R around the deadlock state, such that an initial state can be found in a given arbitrarily small closed bound $\mathcal{B}^r \subset \mathcal{B}^R$ from which the system can leave \mathcal{B}^R .

As shown in Fig. 15(a), define $\mathcal{B}_d^1(r_d) \triangleq \{p \mid \|p - p^1\| \leq r_d\}$ as the ball of radius r_d around the deadlock position of robot 1. The radius r_d is chosen such that: 1) if $\|v^1\| < \frac{2r_d}{h}$ holds, $\|v_k^1\| < \frac{2r_d}{h}$ and $\|u_k^1\| < \frac{4r_d}{h^2}$ also hold, yielding that $\|\Theta_v v_k^1\| < v_{\max}$ and $\|\Theta_a u_{k-1}^1\| < a_{\max}$

where $k \in \mathcal{K}$; 2) if $p_k^i, p_k^i(t-h) \in \mathcal{B}_d^i(r_d)$ holds for $i = 1, 2$ and $k \in \mathcal{K}$, the constraints $a_K^{12T} p_K^1 = b_K^{12} + w^{12}$ and $a_K^{12T} p_K^1 > b_K^{12}$ hold, $k \in \tilde{\mathcal{K}}$, as the deadlock state shown in the proof of Theorem 1.

Thereafter, the motion tendency of underlying robots are analyzed when they are bounded by $\mathcal{B}_d^1(r_d)$ and $\mathcal{B}_d^2(r_d)$. At time $t-h$, consider the vector

$$r_\tau = ((p_K^2(t-h) - p_{\text{target}}^1) \times (p_K^1(t-h) - p_K^2(t-h))) \times (p_K^1(t-h) - p_K^2(t-h)),$$

along which the unit vector is defined as $\tau = \frac{r_\tau}{\|r_\tau\|}$. Consider the planning process at time t , it can be shown that for robot 1, the following holds

$$\begin{aligned} \tau^T \frac{\partial C^1}{\partial p_K^1} \big|_{p_K^1 = p_K^1(t-h)} &= \tau^T \frac{\partial C^1}{\partial p_K^1} \big|_{p_K^1 = p_K^1(t-h)} - \tau^T \frac{\partial C^1}{\partial p_K^1} \big|_{p_K^1 = p_K^1(t-h)} \\ &= \tau^T \frac{\partial C^1}{\partial p_K^1} \big|_{p_K^1 = p_K^1(t-h)}, \end{aligned} \quad (32)$$

where $\tau^T \frac{\partial w^{12}}{\partial p_K^1} = \tau^T \frac{\partial \{a_K^{12T} p_K^1 - b_K^{12}\}}{\partial p_K^1} = \tau^T a_K^{12} = 0$ leads to $\tau^T \frac{\partial C^1}{\partial p_K^1} = \frac{\partial C^1}{\partial w^{12}} \tau^T \frac{\partial w^{12}}{\partial p_K^1} = 0$. Meanwhile, since both $\|\Theta_a u_{k-1}^i\| < u_{\max}$ and $\|\Theta_v v_k^i\| < v_{\max}$ hold for $k \in \mathcal{K}$, (14a) and $p_{\nu_k}^i = 0, \forall k \in \tilde{\mathcal{K}}$ can be derived in a similar way to the proof of Theorem 1. Furthermore, owing to $a_K^{12T} p_K^1 > b_K^{12}$, it can be obtained that $\lambda_K^{12} = 0$. Combining this fact with (14a), the equalities $\frac{\partial \mathcal{L}^1}{\partial p_K^1} = \frac{\partial C^1}{\partial p_K^1} = 0$ and $Q_k(p_K^1 - p_{K+1}^1) + Q_{k-1}(p_K^1 - p_{k-1}^1) = 0$ hold, $k \in \tilde{\mathcal{K}}$. As a result, $p_k^1, k = 0, 1, \dots, K$ are collinear which induces $Q_k \|p_K^1 - p_{k+1}^1\| = Q_{k-1} \|p_K^1 - p_{k-1}^1\|$. Since it has been shown that $\sum_{k=0}^{K-1} \|p_K^1 - p_{k+1}^1\| = \|p_K^1 - p_0^1\|$, it follows that $Q_k \|p_K^1 - p_{k+1}^1\| = 1/\sum_{k=0}^{K-1} \frac{1}{Q_k} \|p_K^1 - p_0^1\|$ and $\|Q_{K-1}(p_K^1 - p_{K-1}^1)\| = 1/\sum_{k=0}^{K-1} \frac{1}{Q_k} \|p_K^1 - p_0^1\|$. Since $\lim_{Q_0 \rightarrow 0^+} 1/\sum_{k=0}^{K-1} \frac{1}{Q_k} = 0$, it further implies that $\|Q_{K-1}(p_K^1 - p_{K-1}^1)\| = 0$ and $Q_{K-1}(p_K^1 - p_{K-1}^1) = 0$ hold. As a result, it can be derived that $\frac{\partial C^1}{\partial p_K^1} = Q_{K-1}(p_K^1 - p_{K-1}^1) + Q_K(p_K^1 - p_{\text{target}}^1) = Q_K(p_K^1 - p_{\text{target}}^1)$. Along with (32), the following relation holds

$$\tau^T \frac{\partial C^1}{\partial p_K^1} \big|_{p_K^1 = p_K^1(t-h)} = Q_K \tau^T (p_K^1(t-h) - p_{\text{target}}^1).$$

As shown in Fig. 15(a), it is evident that the angle between $p_K^1(t-h) - p_{\text{target}}^1$ and τ are larger than $\frac{\pi}{2}$, i.e., both $\tau^T (p_K^1(t-h) - p_{\text{target}}^1) < 0$ and $\tau^T \frac{\partial C^1}{\partial p_K^1} \big|_{p_K^1 = p_K^1(t-h)} < 0$ hold. In addition, $\tau^T a_K^{12} = 0$ holds by definition. Following (16), it can be derived that

$$\tau^T \frac{\partial \mathcal{L}^1}{\partial p_K^1} \big|_{p_K^1 = p_K^1(t-h)} = \tau^T \frac{\partial C^1}{\partial p_K^1} \big|_{p_K^1 = p_K^1(t-h)} < 0.$$

After convex programming, $\tau^T (p_K^1(t) - p_K^1(t-h)) > 0$ is enforced such that the Lagrange \mathcal{L}^1 is decreased, i.e., p_K^1 has the motion tendency alone the direction of τ .

Lastly, as shown in Fig. 15(b), both $\tau_t^T p_K^1 \geq \tau_t^T p_{\text{target}}^1$ and $\tau_t^T p_K^2 \leq \tau_t^T p_{\text{target}}^1$ hold at time t , where τ_t is the unit vector

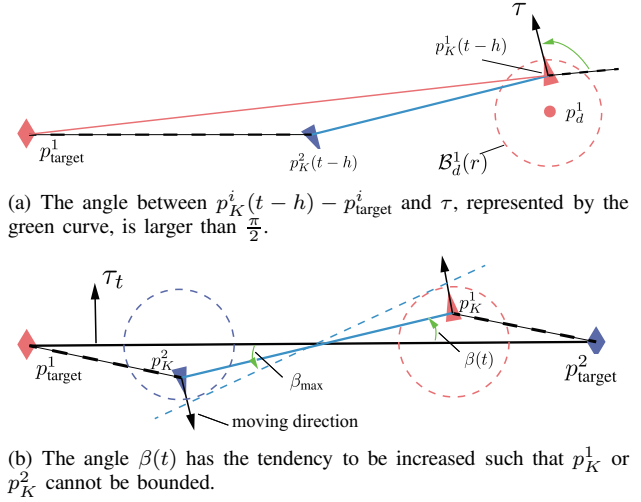


Fig. 15. The deadlock shown in Fig. 5(a) is unstable.

that is perpendicular to $p_{\text{target}}^1 - p_{\text{target}}^2$ at time t . Due to the motion tendency described above, the angle between $p_K^1 - p_K^2$ and $p_{\text{target}}^2 - p_{\text{target}}^1$, denoted as $\beta(t)$ is monotonically increased, i.e., $\beta(t+h) > \beta(t)$ when $\beta(t) \neq 0$. However, the maximum angle β_{\max} is the one associated with the common tangent line of these two spheres $\mathcal{B}_d^1(r_d)$ and $\mathcal{B}_d^2(r_d)$. Thus, starting from any initial state that $\beta(t_0)$ is arbitrarily close to zero, the system will leave the bound $\mathcal{B}_d^1(r_d)$ or $\mathcal{B}_d^2(r_d)$. In other words, the condition of instability imposed in [50] is fulfilled, which completes the proof. \square

REFERENCES

- [1] S.-J. Chung, A. A. Paranjape, P. Dames, S. Shen, and V. Kumar, "A survey on aerial swarm robotics," *IEEE Transactions on Robotics*, vol. 34, no. 4, pp. 837–855, 2018.
- [2] Z. Zhou, J. Liu, and J. Yu, "A survey of underwater multi-robot systems," *IEEE/CAA Journal of Automatica Sinica*, vol. 9, no. 1, pp. 1–18, 2022.
- [3] T. Zhang, J. Xiao, L. Li, C. Wang, and G. Xie, "Toward coordination control of multiple fish-like robots: Real-time vision-based pose estimation and tracking via deep neural networks," *IEEE/CAA Journal of Automatica Sinica*, vol. 8, no. 12, pp. 1964–1976, 2021.
- [4] N. Gafur, V. Yfantis, and M. Ruskowski, "Optimal scheduling and non-cooperative distributed model predictive control for multiple robotic manipulators," in *2021 IEEE/RSJ International Conference on Intelligent Robots and Systems (IROS)*, 2021, pp. 390–397.
- [5] J. Borenstein and Y. Koren, "Real-time obstacle avoidance for fast mobile robots," *IEEE Transactions on systems, Man, and Cybernetics*, vol. 19, no. 5, pp. 1179–1187, 1989.
- [6] Y. Koren and J. Borenstein, "Potential field methods and their inherent limitations for mobile robot navigation," vol. 2, 1991, pp. 1398–1404.
- [7] J. Alonso-Mora, A. Breitenmoser, P. Beardsley, and R. Siegwart, "Reciprocal collision avoidance for multiple car-like robots," in *2012 IEEE International Conference on Robotics and Automation*, 2012, pp. 360–366.
- [8] J. van den Berg, M. Lin, and D. Manocha, "Reciprocal velocity obstacles for real-time multi-agent navigation," in *2008 IEEE International Conference on Robotics and Automation*, 2008, pp. 1928–1935.
- [9] J. van den Berg, S. J. Guy, M. Lin, and D. Manocha, "Reciprocal n-body collision avoidance," in *14th International Symposium on Robotics Research (ISSR)*, vol. 70, 2011, pp. 3–19.
- [10] C. Tomlin, G. Pappas, and S. Sastry, "Conflict resolution for air traffic management: a study in multiagent hybrid systems," *IEEE Transactions on Automatic Control*, vol. 43, no. 4, pp. 509–521, 1998.
- [11] K. Cole and A. M. Wickenheiser, "Reactive trajectory generation for multiple vehicles in unknown environments with wind disturbances," *IEEE Transactions on Robotics*, vol. 34, no. 5, pp. 1333–1348, 2018.

- [12] T. Fan, P. Long, W. Liu, and J. Pan, "Distributed multi-robot collision avoidance via deep reinforcement learning for navigation in complex scenarios," *The International Journal of Robotics Research*, vol. 39, no. 7, pp. 856–892, 2020.
- [13] G. Shi, W. Hönig, X. Shi, Y. Yue, and S.-J. Chung, "Neural-swarm2: Planning and control of heterogeneous multirotor swarms using learned interactions," *IEEE Transactions on Robotics*, pp. 1–17, 2021.
- [14] Y. F. Chen, M. Liu, M. Everett, and J. P. How, "Decentralized non-communicating multiagent collision avoidance with deep reinforcement learning," in *2017 IEEE International Conference on Robotics and Automation (ICRA)*, 2017, pp. 285–292.
- [15] S. Zhao, D. V. Dimarogonas, Z. Sun, and D. Bauso, "A general approach to coordination control of mobile agents with motion constraints," *IEEE Transactions on Automatic Control*, vol. 63, no. 5, pp. 1509–1516, 2018.
- [16] D. Panagou, D. M. Stipanović, and P. G. Voulgaris, "Distributed coordination control for multi-robot networks using lyapunov-like barrier functions," *IEEE Transactions on Automatic Control*, vol. 61, no. 3, pp. 617–632, 2016.
- [17] D. Panagou, M. Turpin, and V. Kumar, "Decentralized goal assignment and safe trajectory generation in multirobot networks via multiple lyapunov functions," *IEEE Transactions on Automatic Control*, vol. 65, no. 8, pp. 3365–3380, 2020.
- [18] A. Richards, J. How, and IEEE, "Decentralized model predictive control of cooperating uavs," in *43rd IEEE Conference on Decision and Control*, 2004, Conference Proceedings, pp. 4286–4291.
- [19] S. El-Ferik, B. A. Siddiqui, and F. L. Lewis, "Distributed nonlinear mpc of multi-agent systems with data compression and random delays," *IEEE Transactions on Automatic Control*, vol. 61, no. 3, pp. 817–822, 2016.
- [20] V. Cichella, I. Kaminer, C. Walton, N. Hovakimyan, and A. M. Pascoal, "Optimal multivehicle motion planning using bernstein approximants," *IEEE Transactions on Automatic Control*, vol. 66, no. 4, pp. 1453–1467, 2021.
- [21] F. Augugliaro, A. P. Schoellig, and R. D'Andrea, "Generation of collision-free trajectories for a quadcopter fleet: A sequential convex programming approach," in *2012 IEEE/RSJ International Conference on Intelligent Robots and Systems*, 2012, pp. 1917–1922.
- [22] D. Morgan, G. P. Subramanian, S.-J. Chung, and F. Y. Hadaegh, "Swarm assignment and trajectory optimization using variable-swarm, distributed auction assignment and sequential convex programming," *International Journal of Robotics Research*, vol. 35, no. 10, pp. 1261–1285, 2016.
- [23] J. Park and H. J. Kim, "Online trajectory planning for multiple quadrotors in dynamic environments using relative safe flight corridor," *IEEE Robotics and Automation Letters*, vol. 6, no. 2, pp. 659–666, 2021.
- [24] W. Hönig, J. A. Preiss, T. K. S. Kumar, G. S. Sukhatme, and N. Ayanian, "Trajectory planning for quadrotor swarms," *IEEE Transactions on Robotics*, vol. 34, no. 4, pp. 856–869, 2018.
- [25] L. Campos-Macias, D. Gomez-Gutierrez, R. Aldana-Lopez, R. de la Guardia, and J. I. Parra-Vilchis, "A hybrid method for online trajectory planning of mobile robots in cluttered environments," *IEEE Robotics and Automation Letters*, vol. 2, no. 2, pp. 935–942, 2017.
- [26] L. Wang, A. D. Ames, and M. Egerstedt, "Safety barrier certificates for collisions-free multirobot systems," *IEEE Transactions on Robotics*, vol. 33, no. 3, pp. 661–674, 2017.
- [27] J. Park, D. Kim, G. C. Kim, D. Oh, and H. J. Kim, "Online distributed trajectory planning for quadrotor swarm with feasibility guarantee using linear safe corridor," *IEEE Robotics and Automation Letters*, vol. 7, no. 2, pp. 4869–4876, 2022.
- [28] J. Alonso-Mora, J. A. DeCastro, V. Raman, D. Rus, and H. Kress-Gazit, "Reactive mission and motion planning with deadlock resolution avoiding dynamic obstacles," *Autonomous Robots*, vol. 42, no. 4, pp. 801–824, 2018.
- [29] J. Grover, C. Liu, and K. Sycara, "Why does symmetry cause deadlocks?" *IFAC-PapersOnLine*, vol. 53, no. 2, pp. 9746–9753, 2020, 21st IFAC World Congress.
- [30] J. Alonso-Mora, P. Beardsley, and R. Siegwart, "Cooperative collision avoidance for nonholonomic robots," *IEEE Transactions on Robotics*, vol. 34, no. 2, pp. 404–420, 2018.
- [31] Y. Zhou, H. Hu, Y. Liu, S.-W. Lin, and Z. Ding, "A distributed method to avoid higher-order deadlocks in multi-robot systems," *Automatica*, vol. 112, p. 108706, 2020. [Online]. Available: <https://www.sciencedirect.com/science/article/pii/S0005109819305692>
- [32] Z. Xing, X. Chen, X. Wang, W. Wu, and R. Hu, "Collision and deadlock avoidance in multi-robot systems based on glued nodes," *IEEE/CAA Journal of Automatica Sinica*, vol. 9, no. 7, pp. 1327–1330, 2022.
- [33] D. Zhou, Z. Wang, S. Bandyopadhyay, and M. Schwager, "Fast, on-line collision avoidance for dynamic vehicles using buffered Voronoi cells," *IEEE Robotics and Automation Letters*, vol. 2, no. 2, pp. 1047–1054, 2017.
- [34] A. Pierson, W. Schwarting, S. Karaman, and D. Rus, "Weighted buffered voronoi cells for distributed semi-cooperative behavior," in *2020 IEEE International Conference on Robotics and Automation (ICRA)*, 2020, pp. 5611–5617.
- [35] M. Abdullhak and A. Vardy, "Deadlock prediction and recovery for distributed collision avoidance with buffered voronoi cells," in *2021 IEEE/RSJ International Conference on Intelligent Robots and Systems (IROS)*, 2021, pp. 429–436.
- [36] K. Garg and D. Panagou, "Finite-time estimation and control for multi-aircraft systems under wind and dynamic obstacles," *Journal of Guidance, Control, and Dynamics*, vol. 42, no. 7, pp. 1489–1505, 2019.
- [37] J. S. Grover, C. Liu, and K. Sycara, "Deadlock analysis and resolution for multi-robot systems," in *International Workshop on the Algorithmic Foundations of Robotics*. Springer, 2020, pp. 294–312.
- [38] J. Grover, C. Liu, and K. Sycara, "The before, during, and after of multi-robot deadlock," *The International Journal of Robotics Research*, vol. 0, no. 0, p. 02783649221074718, 2022.
- [39] H. Zhu and J. Alonso-Mora, "Chance-constrained collision avoidance for mavs in dynamic environments," *IEEE Robotics and Automation Letters*, vol. 4, no. 2, pp. 776–783, 2019.
- [40] Y. Chen, M. Cutler, and J. P. How, "Decoupled multiagent path planning via incremental sequential convex programming," in *2015 IEEE International Conference on Robotics and Automation (ICRA)*, 2015, pp. 5954–5961.
- [41] L. C. E. and A. P. Schoellig, "Trajectory generation for multiagent point-to-point transitions via distributed model predictive control," *IEEE Robotics and Automation Letters*, vol. 4, no. 2, pp. 375–382, 2019.
- [42] K.-D. Kim and P. R. Kumar, "An mpc-based approach to provable system-wide safety and liveness of autonomous ground traffic," *IEEE Transactions on Automatic Control*, vol. 59, no. 12, pp. 3341–3356, 2014.
- [43] B. Kouvaritakis and M. Cannon, *Model predictive control*. Springer, 2016, p. 38.
- [44] S. Boyd, S. P. Boyd, and L. Vandenberghe, *Convex optimization*. Cambridge university press, 2004.
- [45] J. Tordesillas and J. P. How, "Mader: Trajectory planner in multiagent and dynamic environments," *IEEE Transactions on Robotics*, pp. 1–14, 2021.
- [46] S. Diamond and S. Boyd, "CVXPY: A Python-embedded modeling language for convex optimization," *Journal of Machine Learning Research*, vol. 17, no. 83, pp. 1–5, 2016.
- [47] E. D. Andersen and K. D. Andersen, *The Mosek Interior Point Optimizer for Linear Programming: An Implementation of the Homogeneous Algorithm*. Boston, MA: Springer US, 2000, pp. 197–232.
- [48] L. C. E., "Multiagent planning," Website, https://github.com/carlosluis/multiagent_planning.
- [49] D. Mellinger and V. Kumar, "Minimum snap trajectory generation and control for quadrotors," in *2011 IEEE International Conference on Robotics and Automation*, 2011, pp. 2520–2525.
- [50] J.-J. E. Slotine and W. Li, *Applied Nonlinear Control*, 1991.